PROBABILISTIC CHARACTERIZATION OF MECHANICAL PROPERTIES AND RELIABILITY ASSESSMENT OF METAL CASTINGS

BY

IBRAHIM ABDELAZIZ ALI OSMAN

A Thesis Presented to the
DEANSHIP OF GRADUATE STUDIES

KING FAHD UNIVERSITY OF PETROLEUM & MINERALS
DHAHRAN, SAUDI ARABIA

In Partial Fulfillment of the
Requirements for the Degree of

MASTER OF SCIENCE

In

MECHANICAL ENGINEERING

APRIL 2019

KING FAHD UNIVERSITY OF PETROLEUM & MINERALS

DHAHRAN- 31261, SAUDI ARABIA

DEANSHIP OF GRADUATE STUDIES

This thesis, written by **IBRAHIM ABDELAZIZ ALI** under the direction of his thesis advisor and approved by his thesis committee, has been presented and accepted by the Dean of Graduate Studies, in partial fulfillment of the requirements for the degree of **MASTER OF SCIENCE IN MECHANICAL ENGINEERING.**

Dr Sulaman Pashah
(Advisor)

Dr. Zuhair M. Gasim
Department Chairman

Anwar Khalil Sheikh

Dr. Anwar K. Sheikh
(Member)

Dr. Salam A. Zummo
Dean of Graduate Studies

Dr. Jafar Albinmousa
(Member)

8 /Dec /2019
Date

Dedicated to my beloved parents

Abdelaziz & Salwa.

To my brothers & my sisters

Ali, Shima, Mido, Didi & Aboody with love

ACKNOWLEDGMENTS

All praise and gratitude to Allah lord of the worlds who blessed me with the intellect, patience, courage, and strength to achieve this milestone in my life.

This milestone would not have been possible without the support of my family. To my parents, I will be forever grateful for their unconditional love, continuous encouragements, and support throughout my life. A special thanks to my brothers and sisters for their love, moral support and prayers.

I would like to express my appreciation and my honestly gratitude to my advisor Dr. Sulaman Phasha for his support, guidance, patience, and motivation. I thankful for his help during my phases of my master's years. My sincere thanks and gratitude to my thesis committee member Dr. Anwar Sheikh, for his extraordinary support. Also, special thanks to my thesis committee member Dr. Jafar Albinmousa for his assistance and support.

I would like to recognize the invaluable assistance and support from Dr. Muhammed Adinoyi, Dr. Hisham Khogali, my research group colleagues, ME workshop and structural lab in civil department.

I am greatly indebted to my distinguished friends in KFUPM who stand with me and made my stay at KFUPM a memorable journey life, full of joy and happiness.

Finally, I would like to acknowledge KFUPM for providing me with the opportunity to purse my master’s degree

TABLE OF CONTENTS

LIST OF TABLES

LIST OF FIGURES

LIST OF ABBREVIATIONS

ASTM	:	American Society of Testing and Materials
CAD	:	Computer Aided Design
CAM	:	Computer Aided Manufacturing
DOE	:	Design of Experiments
FDM	:	Finite Difference Method
FEM	:	Finite Element Method
FVM	:	Finite Volume Method
JICA	:	Japan International Cooperation Agency
LEFM	:	Linear Elastic Fracture Mechanics
SAE	:	Society of Automotive Engineering
SEM	:	Scanning Electron Microscopy

ABSTRACT

Full Name : [Ibrahim Abdelaziz Ali Osman]

Thesis Title : [Probabilistic Characterization of Mechanical properties and Reliability assessment of Metal Castings.

Major Field : [Mechanical Engineering]

Date of Degree : [April 2019]

In this work we will explore the probabilistic nature of metal cast products. Results from published literature and our own program of testing specimens produce by MAMGAsoft, where optimized mold were used, for mold filling, solidification sequence, stresses and defects prediction in cast products. First, mechanical properties of the cast products were characterized in terms of mean, scatter, and probability distribution for static loading, which was further explored for dynamic loading leading to fatigue failure. Then, relationship between life and strength was explored and probabilistic model for fatigue life in associated with Stress-life curve will be developed.

The micro porosity is the main defect, which is difficult to fully eliminate even in an optimized mold, which has an impact on the life of the cast product. This implication was explored using simple empirical model to define the endurance limit and the ultimate tensile strength as well as stress and cycles to failure.

In the last part of the work, various loading pattern and corresponding probabilistic models were explored to characterize the load or stress distribution. These probabilistic stress models and the strength models developed earlier as a function of operating life were analyzed using stress-strength models to predict the cast part reliability. The developed

simplified approach is compared with results of more sophisticated finite element method (FEM) based analysis from literature

ملخص الرسالة

الاسم الكامل: إبراهيم عبد العزيز علي عثمان

عنوان الرسالة: دراسة عددية وتجريبية للمسامية على المصبوبات المعدنية

التخصص: الهندسة الميكانيكية

تاريخ الدرجة العلمية: ابريل 2019

في هذا البحث سوف نستكشف الطبيعة الاحتمالية للمنتجات المعدنية التي تم سباكتها .نتائج من الدراسات السابقة وبالإضافة لبرنامجنا الخاص باختبار العينات الذي تم اعداده باستخدام برنامج MAMGAsoft، لاختيار القالب الأمثل وفيه ايضا خطوات ملء القالب، وتسلسل التصلب والتنبؤ بالإجهادات والعيوب في المنتجات المصبوبة

.أولاً، الخواص الميكانيكية للمنتجات المصبوبة تم دراسة صفاتها من حيث المتوسط والتباين والتوزيع الاحتمالي للحمل الثابت، وايضا هذه الصفات تم استكشافها ودراستها للحمل الديناميكي الذي يؤدي إلى الفشل والتعب .بعد ذلك، تم استكشاف العلاقة بين العمر التشغيلي والقوة وسيتم تطوير نموذج احتمالي للعمر والإجهاد المرتبطة بمنحنى الإجهاد-الحياة.

المسامية ذات الحجم الصغير هي العيب الرئيسي الذي يصعب القضاء عليه بالكامل حتى في القالب الأمثل وهذا العيب له تأثير على الحياة للمنتج المصبوب .تم استكشاف هذا المعنى باستخدام نموذج تجريبي بسيط لتحديد حد القدرة على التحمل وقوة الشد في نهاية المطاف، وكذلك الإجهاد وعدد الدورات التي تؤدي لفشل المنتج.

في الجزء الأخير من العمل، تم استكشاف أنماط تحميل متنوعة ونماذج احتمالية مماثلة لتحديد خصائص توزيع الحمل أو الضغط .تم تحليل نماذج الإجهاد الاحتمالية هذه ونماذج القوة التي تم تطويرها مسبقًا كدالة للحياة باستخدام نماذج مقاومة الإجهاد للتنبؤ بموثوقية الجزء المصبوب. تمت مقارنة النهج المبسط المطور بنتائج التحليل الأكثر تطوراً لطريقة العناصر المحددة (FEM) من الدراسات السابقة.

CHAPTER 1

INTRODUCTION

1.1 Background

Since early ages, casting process was used to produce products, as example arrowheads, shield and other objects. Casting is widely used as it offer flexibility to produce complex shapes in mass production. Several product are produce by casting process such as pistons, cylinder heads, engine blocks, wheels, etc.[1], [2]

Casting is a process in which metals is melted in the furnace and then the molten metal is introduced through a pouring basin into a perforated cavity, after it solidify it assume the shape of the mold cavity. The mold design in metal casting is built on industrial standards such as ASTM, JICA and SAE. and one of the significant factors is the expertise of the foundry men. The process to design a mold consist of activities in repeated cycles which start from using pattern, design gating and riser system, mold preparation, melting of the metal, pouring process, mold shakeup, heat treatment and post processing and finally quality control and inspection for the cast products.

There are many factors that affect casting starting from the design of the gating system. The solidification process is controlled by selecting and designing the proper gating system to ensure fluid flow during the casting. Usually, it consists of pouring basin,

sprue, gate and well. The riser system, which act as reservoir, provides the required metal to avoid shrinkage caused by solidification of casting.

1.2 Casting Classifications

Processes of casting is classified according to molds into two major categories as:

- Expendable Mold

Generally, it is made of sand, plaster, and ceramics. The expendable-mold processes are grouped according to type of the pattern as permanent or expendable. The permanent pattern includes, Sand casting, Plaster mold casting, Ceramic mold casting and Shell mold casting. The expendable pattern casting category consists of lost foam and Investment casting.

- Permanent Mold

The metallic mold that can sustain the elevated temperature without affecting their strength such as steel, refractory metal alloys or bronze. The major types of permanent mold casting are: Die-Casting, Centrifugal Casting, Slush casting, Pressure casting and squeeze casting. The parts produced by permanent mold methods have higher dimensional accuracy compared to expendable mold, but the cost of equipment and mold is higher [1].

Since our objective is to study the optimized sand mold castings; therefore, the sand casting process, its major defects and affect other casting parameters will now be discussed in detail.

1.2.1 Sand Casting

It is a process that involves the use of a pattern, furnace, sand mold and sprue and runners. The molten metal is poured in the cavity to fill it through gating system to the desired shape that already placed in sand. Engine blocks, cylinder and housing of pumps and motor are just as example of parts that could be casted using sand casting.

Silica Sand is more frequently used in sand casting operation due to its great abundance and a great benefit of sand in manufacturing applications is that sand is inexpensive. There are two types of sand: bank sand which is bonded naturally and lake sand.

1.3 Casting Defects

Following are the major types of the defects that occurred during casting which influence the quality of the casting and reduce the fatigue life [3]–[5].

1.3.1 Porosity

It occurs during the melting and pouring stages by shaping a hollow shape in the metal casting due to dissolution of gases and air entrapment in the molten metal. It could be classified to micro parasite and micro porosity.

Micro porosity usually is difficult to be detected through the (NDE) methods and it is not having a great effect on the stiffness and stress redistribution, while it has higher influence on ductility and fatigue properties [6], [7].

Macro porosity could be defined as the porosity greater than hundred microns and easily visible without need to be magnified. It affects the effective elastic modulus negatively. As consequence of presence of pores, stress-strain redistribution take place and localized

plastic deformation which leads to crack and failure, especially if stress concentration occurs near these pores [8].

1.3.2 Shrinkage Porosity

The contraction of the molten metal during solidification as consequence of lack of the liquid metal required to feed a casting section one reason behind this defect is due to improper design of the feeding system.

1.3.3 Gas Porosity

This gas form voids in metal due to dissolution of gases during cooling.

1.3.4 Pouring Metal Defects

This defect consists of misrun, inclusions and cold shuts. A misrun happens when mold cavities are not filled properly with molten metal.

Inclusions as example dirt and slag that could fall in the molten metal during filling and this dirt solidify inside the casting. The vital reason behind this phenomenon is exposure to the atmosphere and the melt got oxidized. Sand inclusion is considered as the most reasons for rejecting the casting frequently. It occurs due to falling of sand particles into the molten metal and solidifying inside the cast

Cold shut is a weak spot that occurs due to improper fuse or welding of the two streams liquid in the cavity.

1.3.5 Hot Tears:

It is a crack or separation fracture forms during solidification and lead to an unfilled space in the casting to be pulled apart. The reason behind it the insufficient supply of molten metal during the solidification stage.

1.3.6 Hotspots

It is formation of localized cavity due to improper cooling practice and shrinkage effect.

1.4 Motivation

The high demand from market to produce a high quality, quantity cast with the minimum lead time for the design and production and achieving higher casting yield was a challenging process for conventional casting foundries as it needs more trial and errors to accomplish the job. Over the last few decades, many changes in casting industries took place since casting simulation software have been introduced. This lead to obtain acceptance among the manufactures industries and the research area. The use of a software reduces casting defects and improve the quality and the reliability on the cast products [9], [10]. The advancement in computational techniques and numerical simulation tools play a key role in improving casting process and increase the reliability of cast products as it helps in analyzing the mold filling process, solidification process, cooling stage and also predicts the location and types of the most internal defects. Introducing computer aided design and manufacturing (CAD/CAM) accompanied with casting standard led to reduce time, cost needed in product development and allow users to obtain optimum casting geometries while take in consideration filling simulation, analysis of solidification process and the stress distribution inside the cast product.

Casting simulation tools allow researchers and foundrymen to model, optimize the design and process parameters in early design stage before they practice in a foundry, check, and validate the process in a well-organized and economical methods. The incessant development of this tool led to a range of product development process for instance process selection, flow pattern, quality control, design of tooling and stress analysis for the product. Possibility to improve the quality and minimize defects as much as through the simulation and visualization of the filling and solidification behavior and ability to realize and understand the implicit factors affecting product quality and how the defects form during the casting process.

1.5 Thesis Objectives

The main objectives of this thesis are:

1- To study porosity presence on cast steel parts optimized through MAGMAsoft.

2- Develop an empirical model to incorporate the effect of porosity on mechanical properties under static and fatigue loading.

3- Validation of the developed model by comparing its result with experimental test and simulated results reported in literature.

4- Assessing the reliability of the cast product in presence of micro porosity and consequently the scatter in its mechanical properties and loading conditions.

CHAPTER 2

LITERATURE REVIEW

The most vital task for every casting foundry is to deliver a high-quality part as per customer's requirements with minimum cost of production as well as obtaining the maximum yield. One of the most challenging factors that affect the engineers in casting design is casting defect such as porosity, which made difficult to produce a free porosity casting.

Designers need to apply large safety factors to secure the reliability of the cast parts, which will lead to raise the casting weight and make it difficult to be casted or it become unfriendly cast beside the inflation of the cost and the production time and the increase the time needed to develop new products.

Quality of steel casting is determined by conducting nondestructive examination (NDE) methods. These methods use visual examination, dye penetrant testing or magnetic particle to inspect and classify the magnitude of the surface, while volumetric inspection use radiography and ultrasonic examinations.

The needs for using casting simulation tools appears because designers usually face difficulties to relate NDE results to the cast performance.

This chapter presents the different techniques used to predict and simulate the porosity and the effect of the porosity on the cast products using casting simulation software combined with mechanical testing and simulation software.

2.1 Experimental Techniques

Radiographic testing is one of important tools used by quality engineers in foundries to evaluate the quality of the cast and to investigate the porosity presence in the cast, as porosity is one of the important challenges in casting quality.

Hardin and Beckermann [7], [11], [12] used radiographs and X-ray tomography to predict the fatigue life of cast steel components and to measure the porosity in the casting. X-ray tomography in the study was utilized not only to measure porosity, but also to control and rebuild the distribution of porosity. The porosity data obtained from X-rays was mapped to finite element mesh through the three-dimensional quadratic interpolation subroutine. Their results conclude that the stiffness of a porous material depends on the porosity amount, its distribution and the geometry of the pores.

The method of using microCT to characterize the casting and provide a 3D image with details of distribution, shape, and size of all defects despite of prohibitive cost of it in compare to radiographic inspection tools it is used in a large scale. Vanderesse et al. [13] developed an approach based on micro tomography and depend on image analysis method using microCT with combination of finite element analysis tools to investigate the root source of fatigue failure and fracture in the pressure-cast aluminum alloy. They used the volumetric images as an input data for the finite element simulation. The images contain internal porosity data at the beginning state and they were develop a correlation between the stress regions in aluminum castings, geometric parameters and fatigue cracks with pores. In another similar work, Nicoletto et al., [14] used the microCT by to characterize gas and shrinkage pores that occurr in castings and used 3D image for finite element analysis to calculate and compute the stress distributions around gas and shrinkage pores.

du Plessis et al. [15] studied the effect of porosity on mechanical properties of cast titanium using X-ray micro computed tomography (microCT). A finite element analysis was done using VGStudioMax 3.0 software on the microCT data providing a 3D view and quantitative values for maximum stress areas. Their results concluded that the simulated stress around pore location was affected by the pore size and it was correlated with ductility of the samples. The reduction in ductility measuring from the samples were found as the size of the pore increase which result in increasing the simulated stresses in these areas.

Fieres et al [15] described a manner which allows to predict the location at which the first crack occurs and the tensile force needed to initiate the first crack for porous aluminum cast . The method is based on a high-resolution X-ray computed tomography (CT) scan of a part, a subsequent static structural mechanics simulation of the scanned model using software VGSTUDIO MAX by Volume Graphics to reconstruct the material surface from the CT scans, including all internal porosity. Tensile tests were conducted to validate their method using samples produced and manufactured from AlSi10Mg Aluminum alloy.

Slotwinski et al [16] used various techniques to measures the porosity of well-characterized cobalt-chrome samples, their model was built by changing the construction parameters and criteria on a direct metal laser sintering used a commercial additive manufacturing system. They applied different measurement methods for calculating and estimating porosity in their samples. These techniques included X-ray CT, Archimedes and bulk mass and volume methods. For monitoring the porosity variation in metal parts, they introduced an ultrasonic sensor at the time of the fabrication process on a metal powder

bed fusion system. Their results showed an agreement on porosity measurement between these techniques.

2.2 Numerical Techniques and Statistical Methods

YI et al. [17] investigated the influence of porosity on the fatigue life of cast aluminum-silicon alloy. They evaluated it by conducting the high cycle fatigue test on the test specimen with controlled microstructure. They developed a statistical model to establish and build a relationship between the porosity population and the resultant scatter in fatigue life. A Monte-Carlo simulation was done to study and inspect the influence of casting porosity characteristics on fatigue strength in cast aluminum alloys. The inputs of Monte-Carlo simulation were mean pore size, standard deviation, and density of the porosity population, the threshold stress intensity factor of the alloy, together with specimen volume and shape. Based on a model in finite element commercial software ABAQUS, they concluded that pores which were modeled as voids in the model, take the role in initiating the cracks.

Avalle et al. [18] carried out an experimental study using a cantilever rotating bending testing machine to study the effect of casting defects on static and fatigue strength in aluminium alloy casted by high pressure die-cast. The authors used finite element method to reproduce the experimental to get the values high stress in some regions of interest. Their model did not consider incorporating the casting defect.

Yi et al [19]developed a probabilistic model to establish a relationship between the porosity population and the fatigue strength of the cast 319-type aluminum alloy that was evaluated using an ultrasonic testing system. A Monte-Carlo simulation based on this model was

performed to examine the effects of casting porosity characteristics on fatigue strength in cast aluminum alloys.

Ben Ahmed et al [20] studied the reliability of high cyclic fatigue of defective Aluminum alloy by developing Kitagawa diagram probabilistic model. They reported that these approaches introduce a safe method for evaluation fatigue limit in real engineering problems. They used commercial software ABAQUS to combine the finite element analysis (FEM) with Monte Carlo simulation (MCS) method. They built their finite element model based on the assumption that the porosity shape is represented only by spherical shape and using porosity input data from MCS. Different Scenario are simulated numerically by changing loading parameters and porosity size using a nonlinear model. Their proposed numerical model shows a good result agreement with experimental results in obtained fatigue life under different loading.

Dabade et al. [21] studied the defects and analyzed the root cause of these defects in green sand casting using a combination of design of experiments techniques with assistance of casting simulation tools to attain the optimum settings of the molding sand and mold related process parameters, which are the moisture content, permeability of molding sand and mold hardness and green compression strength. The shrinkage porosity was predicted with help of casting simulation software during filling and solidification process. Optimization of casting process parameters to minimize defects was done by using Taguchi method and analysis of variance (ANOVA). The objective was to select the optimum parameters that influence quality of the cast products and reduce rejection percentage. They reported that the rejection rate was diminished to 3.59 percent from initial 6 percent reduction rate.

Bahmani et al [22] studied the micro porosity formation in Aluminum alloy casting by developing a mathematical model stand on finite difference method. They linked between the cooling rate, the content of the gas at the initial state and how the micro porosity is distributed and it is amount in the cast. Their model result showed agreement with data obtained through experimental tests.

2.3 Casting Simulation Software

2.3.1 Introduction to Casting Simulation Software

Although modeling of the casting process is complex process as it affected by many parameters such as pressure, geometry of the mold, fluid velocity and gating system etc, many commercial softwares were come to light over time as consequence of the ability to understand physical phenomena behind casting process. There are many casting simulation software accessible to the foundries industries and researchers such as AutoCast, CastCae, MAGMASoft, ProCAST and Flow-3D Cast etc.

Generally, in the commercial casting software each casting project consists of five steps. Starting from collecting the data and information related to CAD geometry of the model, mold properties, materials properties and parameters needed in the process. Next, CAD part is converted to three-dimensional mold which includes the gating system, runners, cores, risers, feeding system and cavities. Then the boundary conditions should be introduced and after that generating suitable mesh to run the numerical simulation. Post processing module comprise visualization of the results. The casting simulation software allow the users to modify in the design of gating and riser also the parameters and properties

of the material to achieve the optimum design with minimum defects. At the end stage, the all documents of the result are available, in form of images and analysis report etc.

2.3.2 Casting Simulation

Richard and Beckermann [23] have shown the relationship and the dependency of the ductility and the mechanical performance on the porosity amount and the rate of cooling during solidification. Their study reported that the major factors that affect mechanical performance is ductility. The main objective of their study was to search the ability or allowance to use casting simulation outcomes to predict mechanical behavior of cast steel. Micro X-Ray computed tomography was used to compare it with casting simulation result

The same authors [24] used radiographs and tomography to measure . the porosity distribution was measured in the cast part. Their aim was to predict the amount and location of shrinkage discontinuities in steel castings through a simulation model. The simulation was done in commercial software MAGMAsoft. They developed an interface to map the predicted porosity field onto the finite element mesh in ABAQUS to predict the strength and fatigue life of cast steel products. They concluded that the reduction of elastic modulus with the existence of porosity is nonlinear for cast steel they also reported that the distribution, shape and size of pores play a significant role as the quantity of porosity as in the stiffness of the material.

Mahesh et al [25] used Click2cast commercial casting software to study formation of macro porosity in ductile iron cast. Their conclusion is that cooling rate affect shrinkage porosity percentage in the cast and as a result, the rate of porosity increases. They validate their simulation results against radiography results and found an acceptable agreement.

Marek Bruna et al[26] compute porosity that forms during casting process for an aluminum alloys using an advance module for porosity in ProCast casting simulation software. They consider all solidification parameters that affect porosity formation.

G. Unterreiter et al [27] used different softwares to simulate the whole process of manufacturing of Aluminum casting (A356) which includes casting, post heat treatment and machining. MAGMAsoft was used to simulate the die casting process for Aluminum. The output was predicted microstructure and residual stress, which were transferred to other software for studying other properties. They suggested two ways to incorporate the casting simulation results to FEM software. The first one by using MAGMAlink module to FEM software, ABAQUS was used to conduct FEM analysis. An input file in FEM software ABAQUS that contains material definitions, mesh, load, and boundary conditions should be created. This input file and interpolation algorithm were used in MAGMAlink used to transfer results to mesh in FEM software. The second way is with the help of MAGMA API which allow users to access the data through a user interface programming to obtain the mesh data and export it in a text file format. Also, a text file format for the second simulation software (FEM) that contains the mesh information. An in-home software was developed to map the simulation results between the two different meshes.

Dorum et al.[28] carried out a simulation for the casting process of the thin-walled cast magnesium components using the commercial software MAGMAsoft. Their studies aim to study the effect of porosity on the structural behavior of the cast. They transferred the results obtained from the casting simulation software to build a shell element finite element model using LS_DYNA commercial finite element software to study the behavior under quasi-static loading condition.

Richard and Beckermann [29] modeled the casting process for steering spindle cast to predict the porosity using MAGMAsoft. MAGMAlink module was used to map the predicted porosity, which could influence the life of the part, into nodes of a finite element module. Based on the stress analysis result obtained from FEM module, a multi-axial fatigue model was used to forecast the fatigue life of the steering spindle cast. The same authors [30] provided a steel casting with introduce of porosity and through the radiographs they determine the quantity of porosity. This data of porosity obtained from the radiographs mapped into a commercial finite element software ABAQUS using the locally dependence between the elastic properties and porosity. To predict failure behavior and plasticity in ABQAUS, a porous metal plasticity module was used. The results obtained from FEM software were in good agreement with tensile test done the cast.

To predict fatigue life and the crack initiation the Brown-Miller multi-axial strain life model was used, and the predicted stresses obtained from FEM transferred into fatigue software. They compared the predicted fatigue with the measurements obtained from a fatigue test underwent on the cast and obtained the good agreement. As a case study, the same authors used a commercial casting simulation tool MAGMAsoft to predict the porosity defects distribution on a steering spindle casting. The predicted porosity was transferred by use of MAGMAlink module to finite element software. Their objective was to develop an integrated design approach that is a combination of casting simulation with through a finite element software to predict the mechanical performance.

Olofsson and Svensson [31] developed a software to incorporate the casting simulation software MAGMAsoft predication into a finite element method. They developed a user interface in ABAQUS to control their software which was implemented base on Python

programming language. The software is used to define the materials and initial conditions in finite element method software. A test case of ductile iron component was carried to validate the software.

2.4 Summary of the Literature Review

Literature review and studies above provide details on the significant role of casting simulation tool being utilized in enhancement of casting process and rising quality of cast products in the modern foundries. Elimination porosity completely from casting products is a difficult process, and it need more trials and experience to be predicted and linked with casting quality by using traditional tools. However, using casting simulation tool allows to predict porosity as it capable to simulate the effect of changing many casting parameters for instance riser design, gating and runner system design and pouring time etc. many attempts in literature to optimize casting parameters by using design of experiments methods and numerical techniques to decrease porosity effect.

There are efforts in prediction, mapping porosity field obtained by using casting simulation software to FEM software to study the porosity effect in the life of part in service. Table 2.1 show summary the techniques used in predication porosity and the mapping of porosity through using casting simulation software.

Table 2.1 Summary of Literature Review.

Authors	Casting Simulation tools	NDE techniques	Numerical techniques & Statistical Methods	Mapping porosity through the casting simulation tools to FEM	Notes on other way used to mapping porosity to FEM
M.Avalle et al				No	It was not included in the model
Hardin and Beckermann		Yes		No	X-ray was used
Vanderesse et al		Yes		No	X-ray was used
Nicoletto et al.		Yes		No	MicroCT was used
du Plessis et al		Yes		No	MicroCT was used
J.Fieres et al		Yes		No	MicroCT was used
Slotwinski et al		Yes		No	It was not included
Yi, J. Z. et al			Yes	No	Assuming pores as voids in FEM
Ben Ahmed et al			Yes	No	Use Monte Carlo simulation data with assumption of pores as spherical defects
Yi, J. Z. et al			Yes	No	It was not included
Bahmani et al			Yes	No	It was not included
Dabade et al	Yes		Yes	No	
Mahesh et al	Yes			No	It was not included
Marek Bruna et al	Yes			No	It was not included
Hardin and Beckermann	Yes	Yes		Yes	
G. Unterreiter et al	Yes			Yes	
Dorum et al	Yes			Yes	
Olofsson and Svensson	Yes			Yes	
M.A.Khan	Yes			Yes	

CHAPTER 3

OPTIMIZED MOLD

3.1 Introduction

This chapter introduces the optimized mold to produce the cast specimens in order to meet the objectives of the present work. The optimized mold was developed earlier by Khan [32]. The mold is based on the casting simulations using MAGMASoft. The parts are standard specimen parts for both fatigue and tensile tests. Multi-cavity molds are designed to attain uniformity in multiple cast parts [32].

3.1.1 MAGMAsoft for Casting Simulations

The software is built, standing on the base of Finite Difference Method (FDM) and can predict the casting process quality by simulating the mold filling solidification, cooling and has the ability to predict microstructure formation and distribution of the properties

3.1.2 Simulation Steps in MAGMAsoft

The simulations consist of five stages which are gathering of casting data, methods design, Mesh, Definition, methods optimization, and results.

Gathering the data required information related to CAD model of casting, cast metal properties, mold properties, process parameters. Methods design and modeling: in this stage the as cast part model is converted into a (3D) mold which contains cavities, gating

system, runners, risers, cores, and feed. Then generating the optimum mesh and defining boundary conditions. At the end solving and numerical simulation to get results with more flexibility and ability to control parameters that affect the process efficiency and controlling defects.

3.1.3 Cast Parts and Material

The standard tensile and fatigue test specimens are considered as a casted product. Figure 3.1 shows the details of these cast parts.

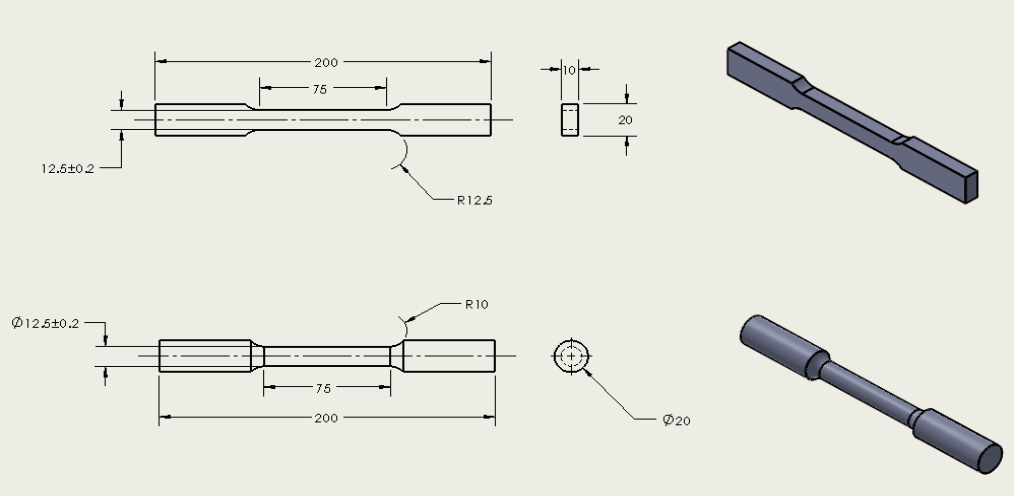

Figure 3.1 The Rectangular Specimen for Tensile Test on Top, The Round for Fatigue Testing on Bottom.

The casted material is ASTM A216 WCB cast steel that is widely used in foundries for casting variety of engineering application. Tables 3.1 and 3.2 show the chemical composition and mechanical properties of the cast steel.

Table 3.1 Chemical Composition in Weight Percentage.

Fe	C	Mn	P	Si	S	Ni	Mo	Cr	Cu
96.2	0.3	1	0.035	0.6	0.35	0.5	0.2	0.5	0.3

Table 3.2 Mechanical Properties.

Yield Strength	248 MPa
Tensile Strength	485MPa
Elongation	22 %

3.2 The Optimized Mold Design

An initial mold is designed according to casting standards and foundry practice. The casting process for the mold is then simulated using MAGMAsoft. MAGMAsoft database properties were used for the sand and core material as well as heat transfer coefficients and other properties. The initial design showed some porosity in the casting. Then they used optimization module in MAGMAsoft with assistance from in-house foundry men, specialized mold designer, to minimize defects in their initial cast. The modifications in the cast layout were made by modifying gating system to minimize friction in the flow, prevent heat loss and produce cast specimen without hotspots defect in the steel specimen. Moreover exothermic sleeves were included [33]–[35]. Figure 3.2 & 3.3 show the CAD model for the final optimized casting layout.

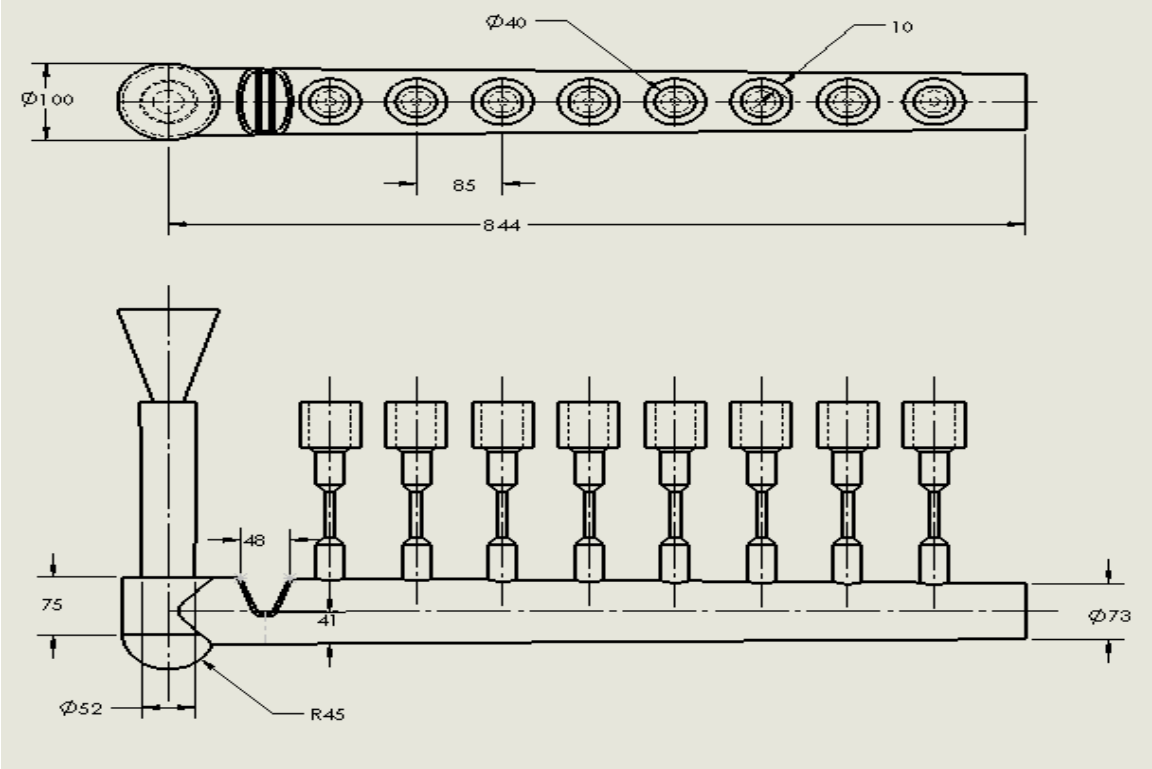

Figure 3.2 The Optimized Casting Layout for Tensile Testing Specimens [32]**.**

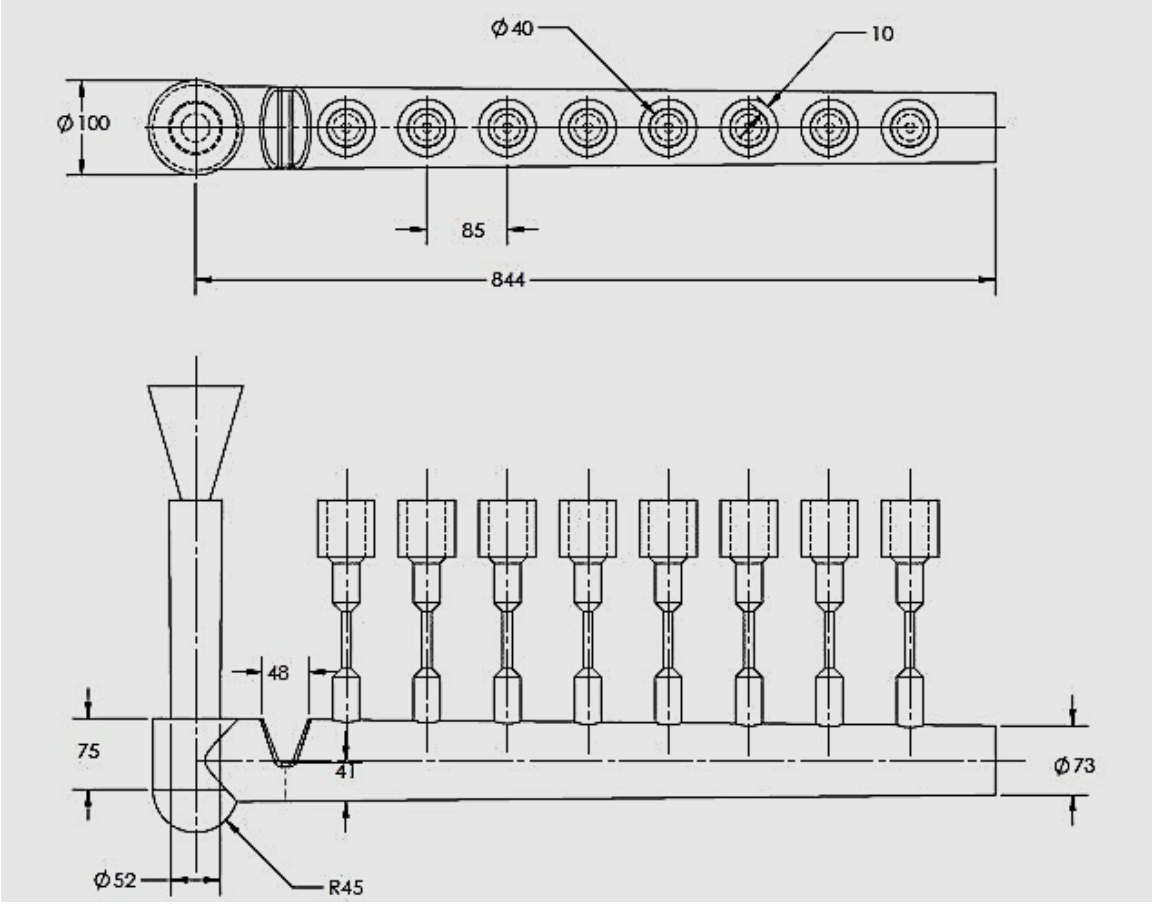

Figure 3.3 The Optimized Casting Layout for Fatigue Testing Specimens[32]**.**

The simulations were then run with the optimized molds and the results are shown in Figure 3.3. The results showed almost the same level of micro porosity in all specimens. However, the porosity in some specimen was observed in grip portion of the specimen.

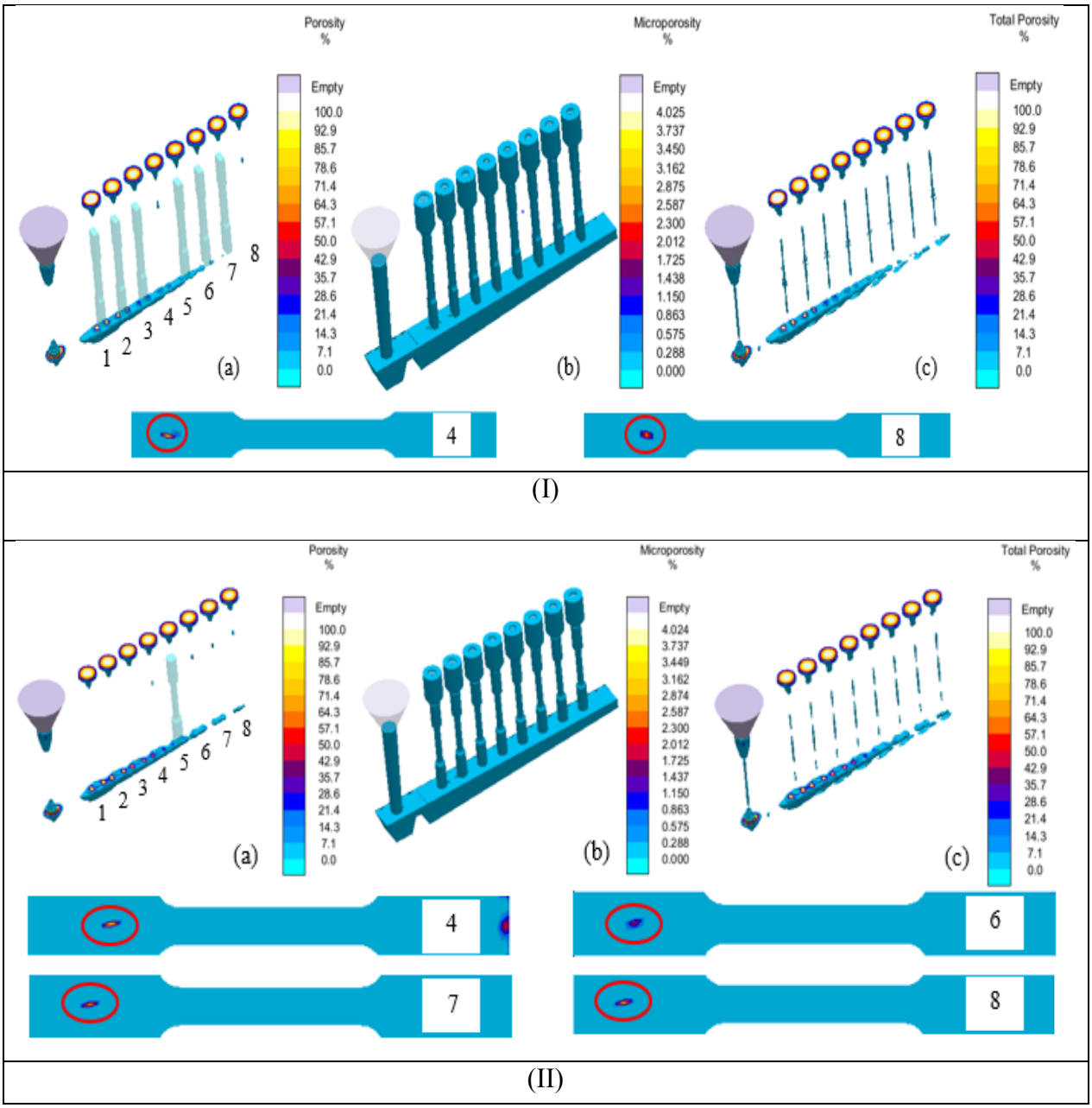

Figure 3.4 Porosity Predicted by using Optimized Mold in MAGMAsoft in X-ray views of (a) Porosity, (b) Micro porosity and (c) Total porosity. (I) Tensile Specimens (II) Fatigue Specimens [32].

3.3 Manufacturing of Tensile and Fatigue Specimens

The actual casting using optimized mold design was done in MASABIK foundry. The castings from the multi cavity molds are shown in Figure 3.5.

a b

Figure 3.5 Wooden Pattern for (a) Tensile Testing Specimens Mold (b)Fatigue Testing Specimens Mold [32].

All tensile and fatigue specimens are normalized, soaked for 30 minutes following that cooling in air at MASABIK foundry after casting. The tensile specimens are then machined based on tensile standard dimension according to ASTM E8[36] and fatigue specimens depend on the fatigue standard dimension according to ASTM E466 [37]. The machined specimen were then heat treated according to ASTM standard in [38].

CHAPTER 4

MECHANICAL TESTING OF CAST SPECIMEN

4.1 Radiographic Test for Porosity

The simulation results of the optimized molds showed that the micro porosity is not completely eliminated. Therefore, prior to conduct and preform mechanical tests for cast specimens, the radiographic X-ray imaging for all the tensile and fatigue specimens is done according to ASTM E466 [37]. The objective is to evaluate and characterize the quality of the cast specimens and to characterize casting defects existing in the cast through radiographic examination. Result obtained for tensile specimens as shown in Figure 4.1 and 4.2 reveals that no visible traces of any considerable or significant porosity. However, in case of fatigue specimens a difference between test section and grips section in appearance is observed as shown in Figure 4.3 and 4.4. On the other side when compare X-ray images with bulk density method which is used to measure porosity in the actual casting it shows that X-ray image cannot detect porosity in micro-scale porosity due to limitation in equipment used to produce X-ray images in current work.

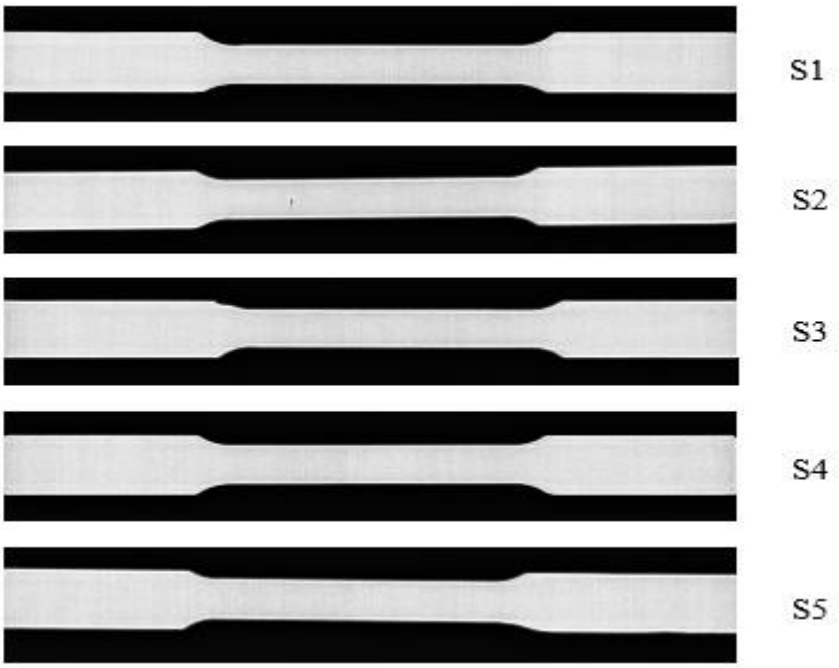

Figure 4.1 X-ray Image of Tensile Specimen [32]**.**

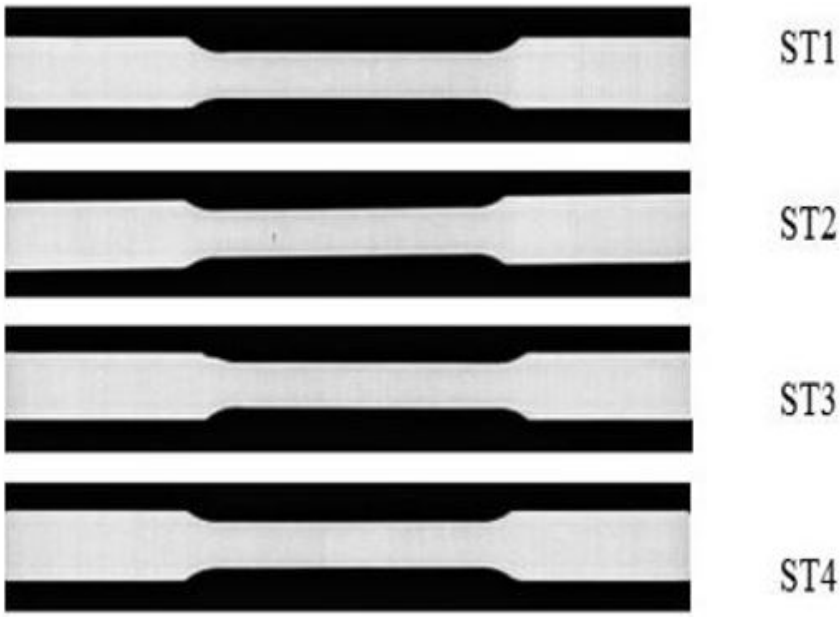

Figure 4.2 X-ray Image of Tensile Specimen.

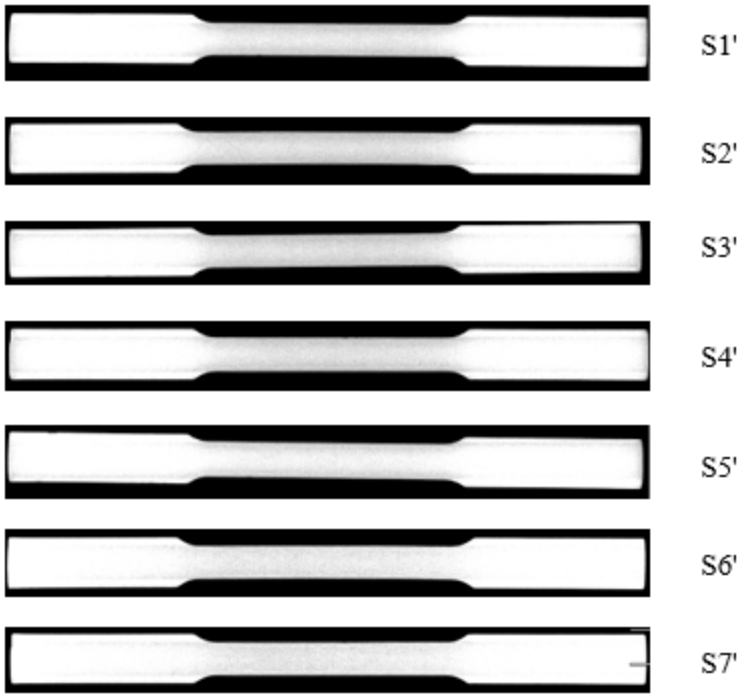

Figure 4.3 X-ray image of fatigue Specimen [32]**.**

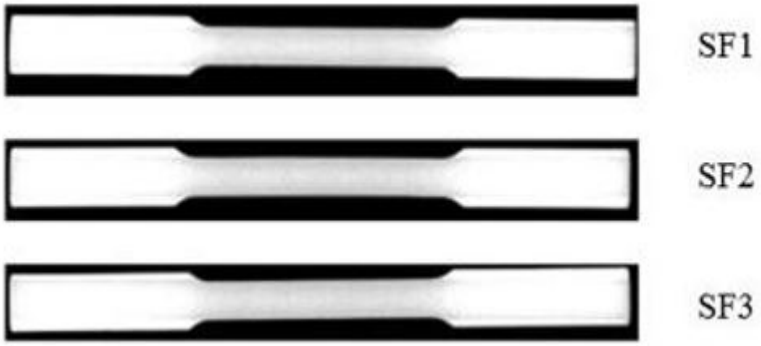

Figure 4.4 X-ray Image of Fatigue Specimen.

4.2 Fractography and Microscopy Examinations of Specimen

The specimen fracture surfaces were examined with the aid of using scanning electron microscope (SEM) following the tensile testing. The examination result in Figure 4.5 revealed that basically no fatigue regions also it displayed very rough and jagged fracture surfaces. These are like the monotonic fracture surfaces, were broadly covered with

ductile dimples as exhibited in the same figure. This microvoid coalescence is typically linked with ductile fracture.

The micropores were observed in a roughly spherical shape as shown in Figure 4.6 with diameter approximately 20 μm.

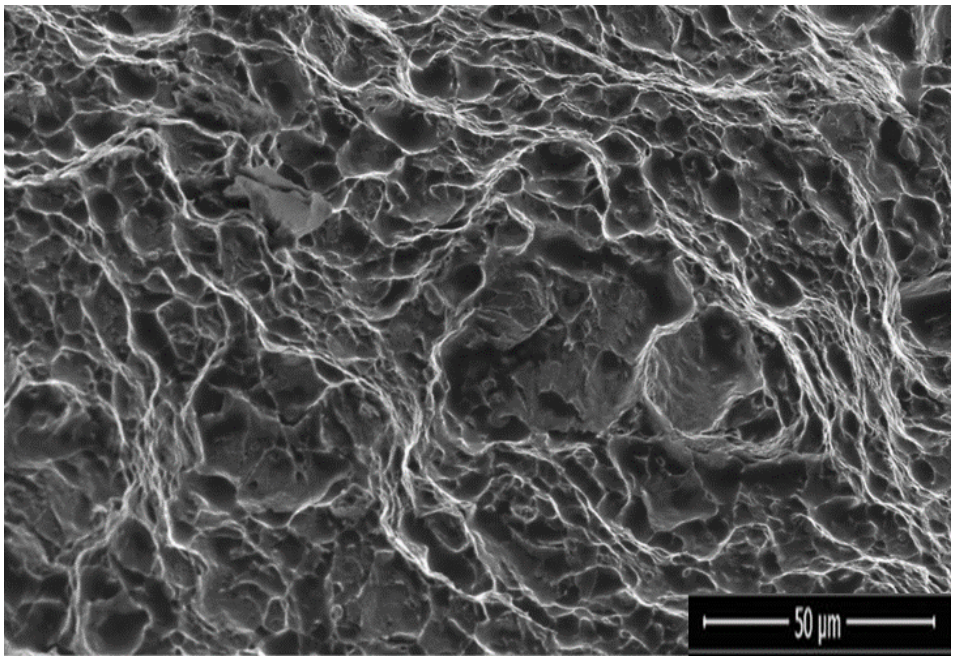

Figure 4.5 Ductile Dimples were Found Typically in The Specimen Fracture.

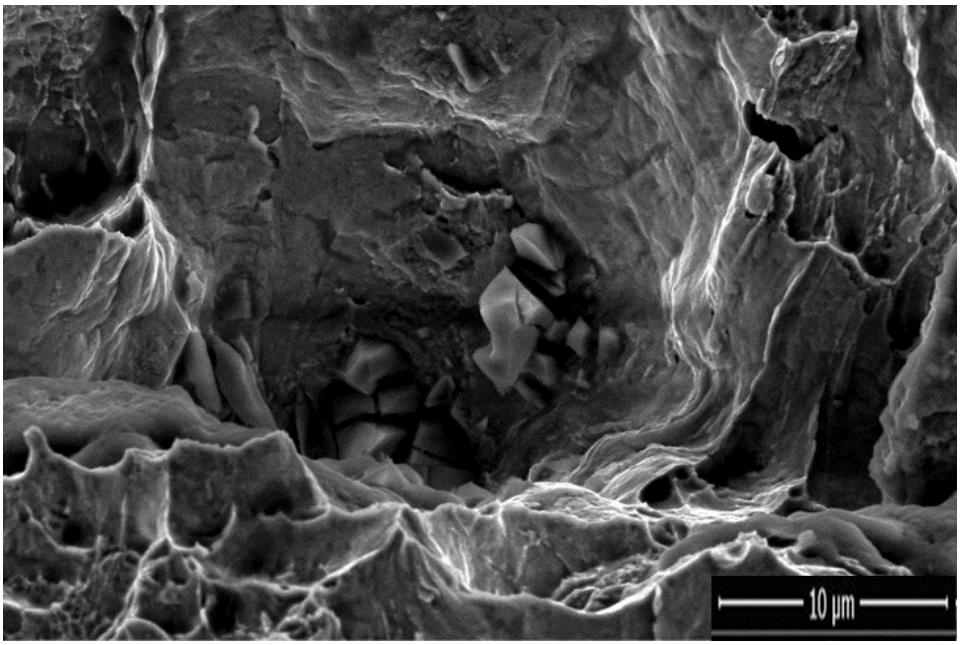

Figure 4.6 A Micropore Near the Surface.

4.3 Mechanical Tests

4.3.1 Tensile Testing

To investigate the monotonic properties, five specimens are selected to conduct tensile test in Instron Universal Testing machine as shown in Figure 4.6. A constant displacement rate of 1 mm per min is used to conduct the test. An extensometer is used for recording the strain resulted from the test.

Figure 4.7 Tensile Test Setup for Tensile Cast Specimen.

The results obtained from tensile test are presented in Figure 4.6 and summarized in Table 4.1. The results are compared to the results of a sound benchmark specimen. The sound specimen does not contain any micro porosity as it was made from roll steel at MASABIK foundry. The results demonstrate that the properties of the cast specimens are somewhat less than the sound specimen due to presence of micro porosity.

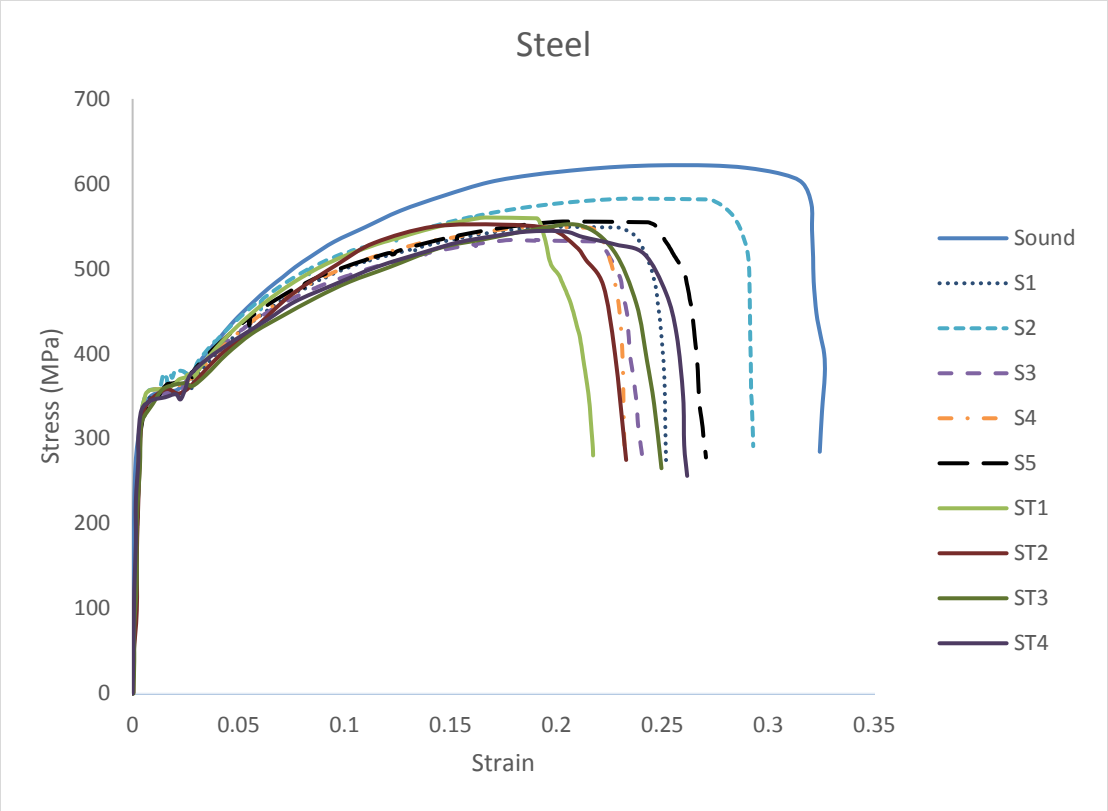

Figure 4.8 Tensile Test Results for Cast Dpecimens, S1 to S5 [32]**, Remaining ST1 to ST4 is the Author Results.**

Table 4.1 Summary of Tensile Test Experiment Results.

Specimen I. D	Yield Strength (MPa)	Tensile Strength (MPa)	Modulus of Elasticity (GPa)	Fracture Strength (MPa)	Elongation (%)
MASABIK Sound steel	355	620	198	293	32.5
S1	340	549	193	275	25.2
S2	355	583	196	292	29.3
S3	337	534	191	267	23.2
S4	356	549	196	275	23.2
S5	347	556	191	278	27
ST1	339	560	191	277	21.7
ST2	341	552	194	275	23.1
ST3	342	551	193	265	24.9
ST4	348	544	195	287	26.1

4.3.2 Fatigue Test

All fatigue tests are conducted using in Instron universal machine, as shown in Figure 4.9, under fully reversed stressing (R = -1). The frequency of the test is selected to be 5 Hz based on the amplitude of the nominal stress of the testing and the load-controlled testing mode is selected.

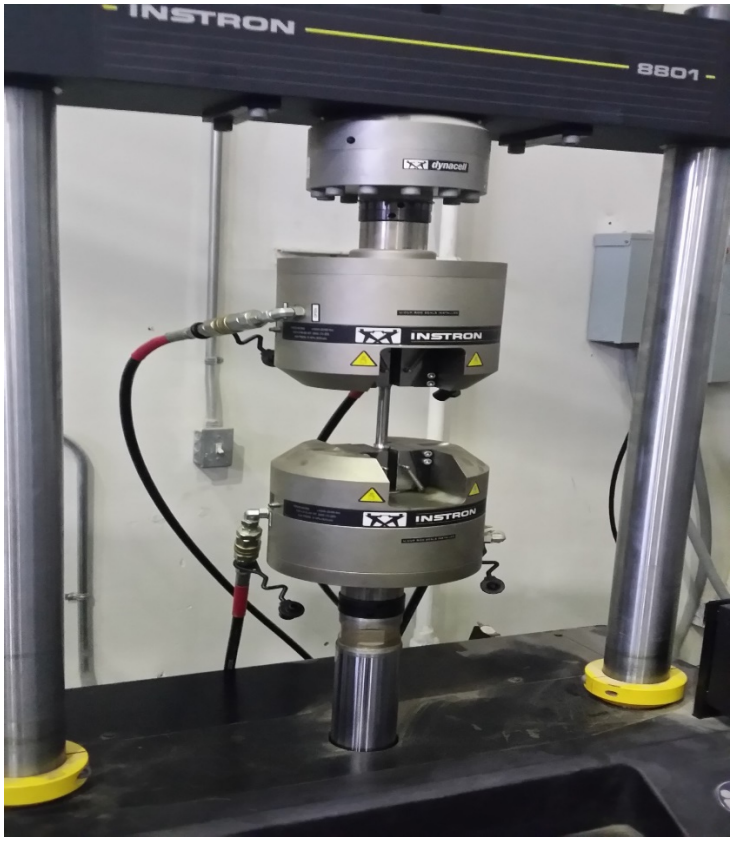

Figure 4.9 Instron Fatigue Test Machine.

The specimens underwent cyclic loading until fracture. The results are summarized in Table 4.2 and presented in form of SN diagram in Figure 4.10. In The S-N curve, the dot circles are the data generated by Khan and additional three data shown in a different color are generated at fix stress level to study the scatter in fatigue life due to micro porosity.

Table 4.2 Summary of Fatigue Test Experiment Results.

Specimen I. D	Stress used for the test (MPa)	Predicted fatigue life (Cycles)
SF1'	326	62
SF2'	244	6,545
SF3'	204	20,561
SF4'	163	56,893
SF5'	122	145,089
SF6	81	535,564
SF7	41	3,061,195
SF1	122	92,218
SF2	122	133,578
SF3	122	216,687

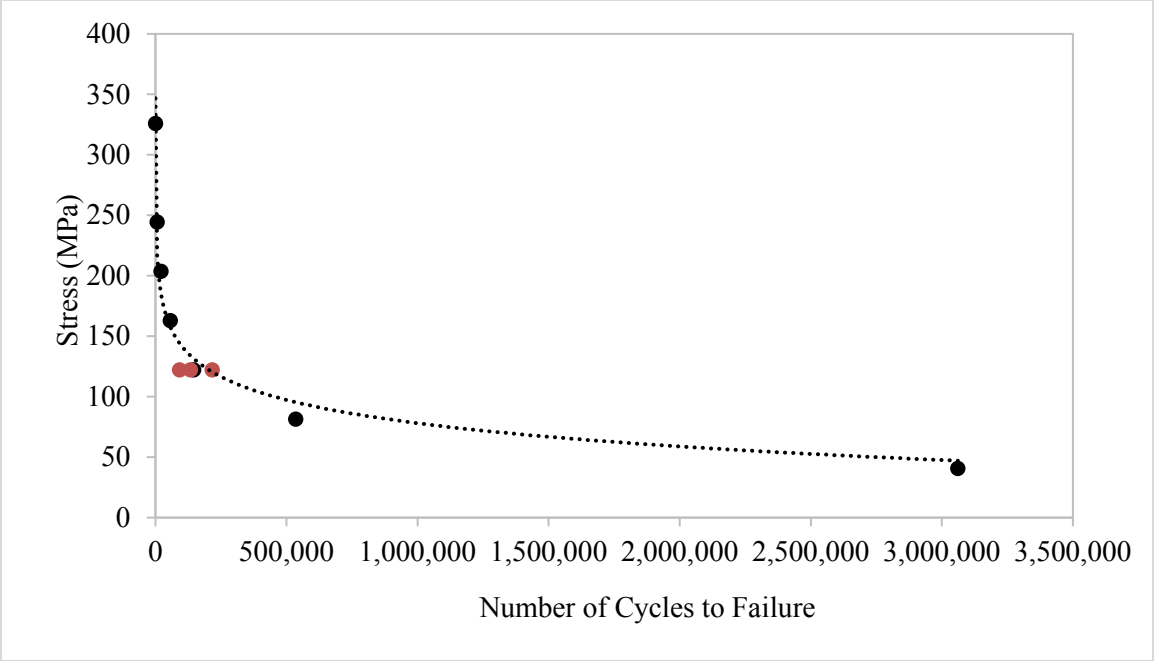

Figure 4.10 S-N curve for cast specimen [32]**, the red dots are the author results.**

4.3.3 Fatigue Results of a Sound Specimen

The sound specimen fatigue results could not be found in the published literature. The following section describes how a theoretical SN diagram for the sound specimen is established.

The fatigue failure could be classified to low-cycle fatigue in which failure takes place starting from one cycle up to one thousand number of cycles and it can be represented in a semi-log plot as in equation 4.1.

$$S = S_{UTS}\, N^{(\log f)/3} \quad (4.1)$$

where:

S_{UTS} : the ultimate tensile strength

f: the fatigue strength fraction, it is defined as in equation (4.2)

$$\boldsymbol{f = \frac{S_{10}{}^{3}}{S_{UTS}}} \qquad (4.2)$$

The next zone is called high cycle fatigue [39]. This ranges from one thousand to one millions cycles to failure. The corresponding equation is as follows:

$$\boldsymbol{S = a\, N^{b}} \qquad (4.3)$$

The values for *a* and *b* are calculated as shown below in equation (4.4) & (4.5) respectively [39]:

$$\boldsymbol{a = \frac{(f\, S_{UTS})^{2}}{S_e}} \quad (4.4)$$

$$\boldsymbol{b = -1/3\ log\left(\frac{f\, S_{UTS}}{S_e}\right)} \quad (4.5)$$

S_e is the endurance limit of the material and the value of S_e either it computed by conducting a laboratory experiment or through an approximate relationship as in [39] where

$$S_{\acute{e}} = \begin{cases} 0.5S_{UTS} & S_{UTS} \leq 700\ MPa \\ 700\ MPa & S_{UTS} \leq 1400\ MPa \end{cases} \quad (4.6)$$

The theoretical S-N curve for sound steel is developed as shown in Figure 4.12 based on values for steel obtained from Table 4.2 where *f* is estimated from figure 4.11 [39] and equations listed above where used to calculate the endurance limit and the ultimate tensile strength is obtained from Table 4.1

Table 4.3 Values for Sound Steel.

S_{UTS}	620 MPa
$S_{endurance}$	310 MPa
f	0.855

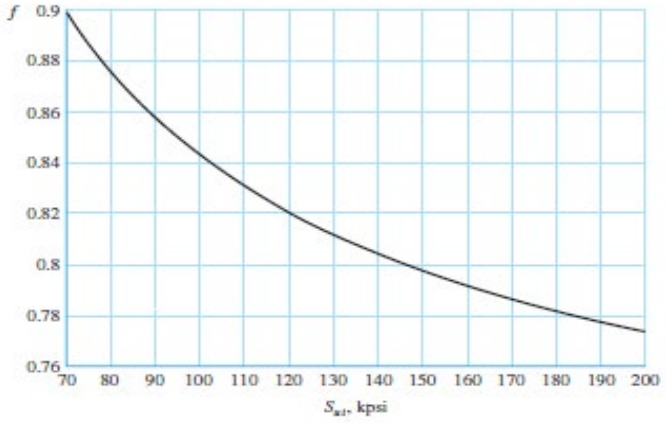

Figure 4.11 Fatigue strength fraction (f) of Suts at 1000 cycles [39]**.**

The S-N curve which is developed after conducting the fatigue test as shown in Figure 4.12 is built on by subjecting six specimens to cyclic load until fracture for finite life and one specimen for infinite life where the life measured is exceed the runout criterion which is for instance 1×10^6cycles in the current work.

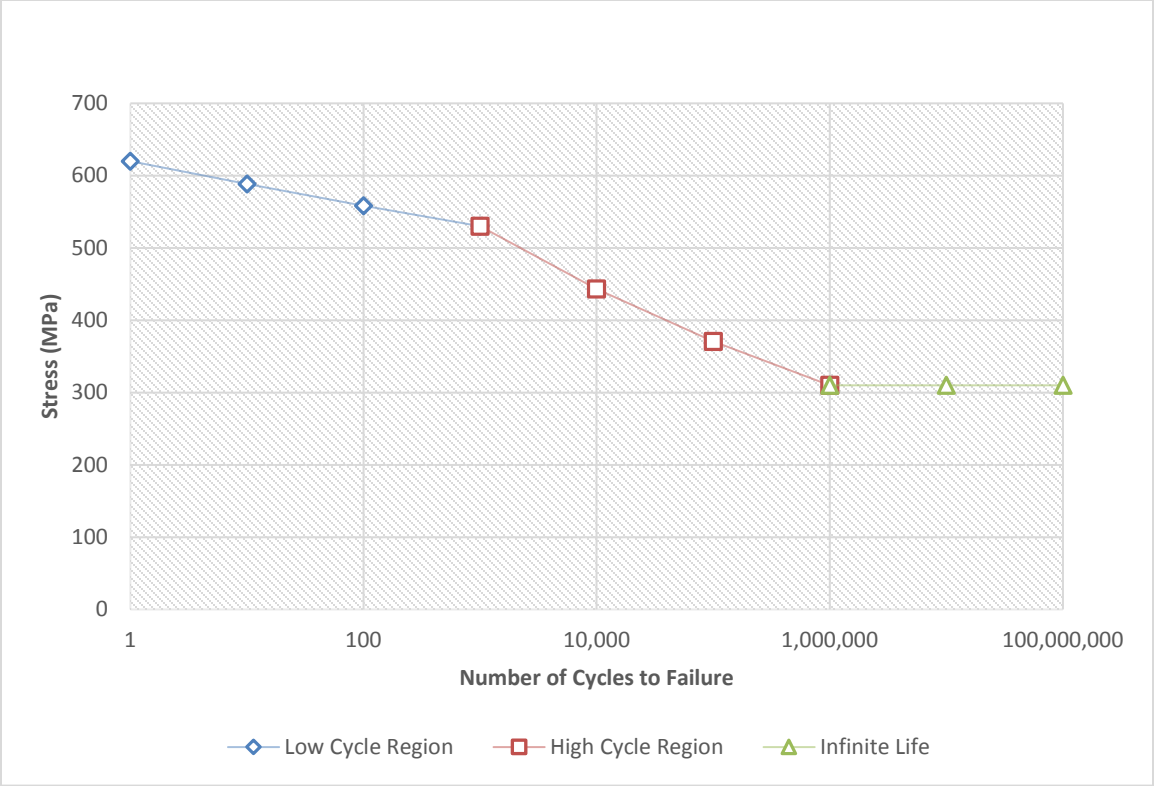

Figure 4.12 Theoretical S-N curve for Sound Material.

CHAPTER 5

STATISTICAL ANALYSIS

The objective of this chapter is to analyze the effect of micro porosity on static and fatigue strengths of the cast specimen. The effect was observed from the experimental results presented in the previous chapter. The analysis approach available in the literature is the one adopted by Hardin et.al [8], [24], [40], [41] and Khan[32]. It is based on tracking the micro porosity in each of the specimen individually. The approach is very useful for a detailed analysis, nevertheless, it requires an in-depth understanding and application of the casting simulation and linking between casting and finite element software for the prediction of fatigue life. Moreover, this cannot be used for a quick engineering calculation.

Indeed, there is an inherent possibility of scatter among cast part due to change of casting condition like temperature, cooling rate, etc. Therefore, our approach will differ from the detailed analysis approach, as we will look at these results as a realization of stochastic process in static and dynamic domain rather than looking at individual test results and mapping it with its porosity. Our view will be for the collection of all curves as a spectrum of multiple realization of random process, which has properties distributed as a collection of identical specimens. Thus, the idea is to conduct a probabilistic characterization of these curves. The developed statistical approach would be validated against the detailed analysis results obtained by Khan [32] and Hardin [24].

In the area of statistics, we collect the data to analyze it and then represent this data to ease the decision making for the sake of solving our complex problem [43]. It is also considered

to be the science of data analysis, data collection, and data interpretation [44]. The part of statistics that aims to understand variability is called statistical method. Moreover, variability in this sense means the differentiation in outcomes between the observed event and exact outcomes.

5.1 Random Variables and Statistical Properties

In this chapter, we are going to treat the static mechanical properties such as yield strength, ultimate tensile strength and elongation as random variables defined as X. A random variable is a real number corresponding to the outcome of a nondeterministic experiment. It can be characterized by statistical parameters, often the mean and variance, and a distribution function, whether assumed or goodness-of-fit tested. These statistical parameters will be covered in the following, as it will be used to characterize the static and dynamic properties obtained through experimental conducted earlier.

5.1.1 Cumulative Distribution Function (CDF)

A way to describe the probability distribution of a random variable is to define a function (of a real number x) that provides the probability that X is less than or equal to x. CDF is a continuous random variable X with probability density function F(x) is

$$\boldsymbol{F(x) = P(X \leq x)} \quad (5.1)$$

5.1.2 Probability Density Function (PDF)

The probability distribution or simply distribution of a random variable X is a description of the set of the probabilities associated with the possible values for X. To obtain f(x) a continuous random variable X is used to determine probabilities as follows:

$$\boldsymbol{Area = P(a \leq X \leq b)} \quad (5.2)$$

Probability plotting is a graphical method for determining whether sample data conform to a hypothesized distribution based on a subjective visual examination of the data.

5.1.3 Central Tendency

The part of statistics that explains the interaction and interdependencies between variables in a community, and shapes the data in the way of mean, median and mode is known as descriptive statistics [42]. In Inferential statistics [42], we try to illuminate a population by using a random sample out of that population. There are two important main concepts in descriptive statistics. The first is central tendency, which describes the level of clustering of observations around a central location. The second is degree of dispersion, which describes spread towards limits [43].

Measures of central tendency is the measures of central tendency are mean, median and mode. Mean is the summation of all the scores divided by the number of scores. The sample mean is the average value of all the observations in the data set. The following formula is used to calculate the mean

$$\boldsymbol{Mean} = \bar{\boldsymbol{x}} = \frac{\sum \boldsymbol{x}}{\boldsymbol{n}} \quad (5.3)$$

where x = each observation & n = number of observations

5.1.4 Variance

Variance is a quantification of the narrowness of a certain distribution. To simplify the explanation of the data, we use the square root of variance. For a specific population, the standard deviation is the square root of the variance, and it can be calculated using the following formula

$$S = \sqrt{\frac{\sum[x_i - x]^2}{n-1}} \quad (5.4)$$

Since material properties have a considerable variability around their nominal value they can best be characterized by some appropriate probability distributions. These distributions represent the dispersion in the respective property of material within a range of values. For analytical decision making these distributions can modelled by continuous probability density functions or probability models.

5.2 Probability Functions for Well-known Distribution

Some of the commonly used probability distributions in characterizing variability of material properties are Normal Distribution, Log-Normal Distribution, and Weibull Distribution. Each distribution has its probability density function which are offered in the succeeding sub-sections.

5.2.1 Normal Distribution

The normal distribution is represented by its famous bell shape and is symmetrical about its mean value. The probability density function is given by

$$f(\mathrm{x}) = \frac{1}{\sigma\sqrt{2\pi}} exp\left[-\frac{1}{2}\left(\frac{\mathrm{x}-\mu}{\sigma}\right)^2\right] \text{ where } \sigma, \mu > 0 \quad (5.5)$$

where, μ is the mean and σ is the standard deviation

5.2.2 Log-normal Distribution

The log-normal probability density function is given by

$$f(\mathrm{x}) = \frac{1}{\sigma_y\sqrt{2\pi}} exp\left[-\frac{1}{2}\left(\frac{\ln x - \mu_y}{\sigma_y}\right)^2\right] \quad (5.6)$$

$$\mu_y = ln\mu_x - ln\sqrt{1 + {C_x}^2}$$

$$\sigma_y = \sqrt{\ln(1 + {C_x}^2)}\,, where\ x \geq 0$$

where, $-\infty<\mu<\infty$ and $\sigma>0$.

5.2.3 Weibull Distribution

The Weibull probability density function is given by

$$f(\mathrm{x}) = \frac{\beta}{\delta}\left(\frac{\mathrm{x}}{\delta}\right)^{\beta-1} exp\left[-\left(\frac{\mathrm{x}}{\delta}\right)^{\beta}\right], where\ x > 0$$

where, β is the shape parameter, and (δ) is the scale parameter, and both are always positive

5.3 Characterizing of Static Properties

In next subs-sections these properties yield strength, ultimate tensile strength, elongation, and hardness are characterized from a probabilistic point of view.

5.3.1 Yield Strength

Table 5.1 show statistical summary for yield strength obtained through conducting experimental test for the cast specimens

Table 5.1 Statistics Summary for Yield Strength.

Average	345.0
Standard deviation	6.9282
Coefficient of variation	2.00817%
Standard skewness	0.841662
Standard kurtosis	-0.585889

Yeild strength results obtained above demonstrated a very small variation about 2.00% (0.02). This also was reflected on Figure 5.1. So, from yield point of view product is quite consistent. Therefore design can use average yield strength

For safe design $\frac{Yield\ strength}{Stress} > 1$

Probability model for yield strength can be Normal, Lognormal or Weibull distribution as they all show P-value more than 0.05 which is demonstrated in the goodness of fit test Kolmogorov-Smirnov Test in Table 5.2. The test determines whether this experimental result obtained from calculating yield strength can be adequately modeled by different distributions. Figure 5.1 display the probability plot for the models proposed to characterize yield strength.

Table 5.2 Goodness-of-Fit Tests, Kolmogorov-Smirnov for Yield Strength.

	Normal	Lognormal	Weibull
DPLUS	0.223054	0.221317	0.278368
DMINUS	0.147765	0.147159	0.193785
DN	0.223054	0.221317	0.278368
P-Value	0.761762	0.770097	0.499538

Table 5.3 gives the summary for the proposed distribution which are displayed in figure 5.2 for the Normal, Log-normal and Weibull distribution respectively

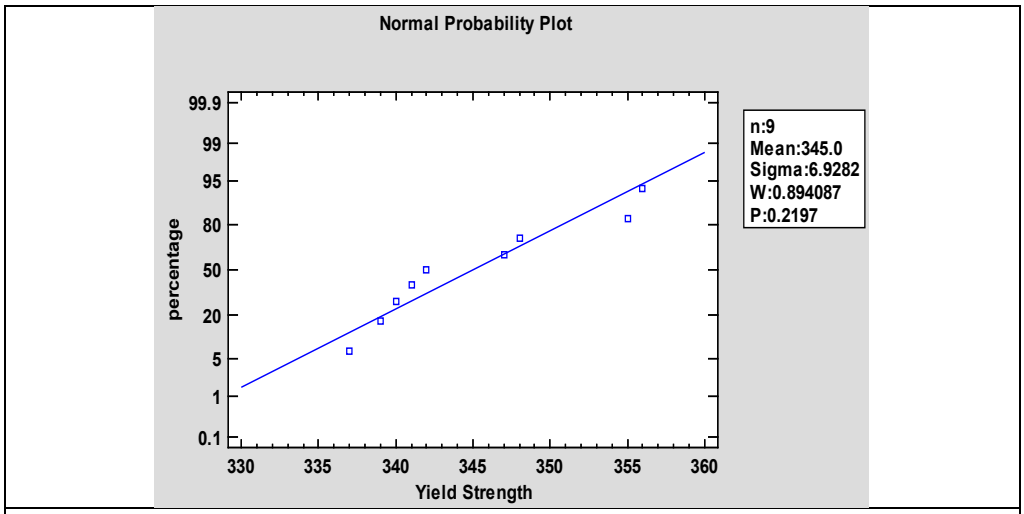

(a)

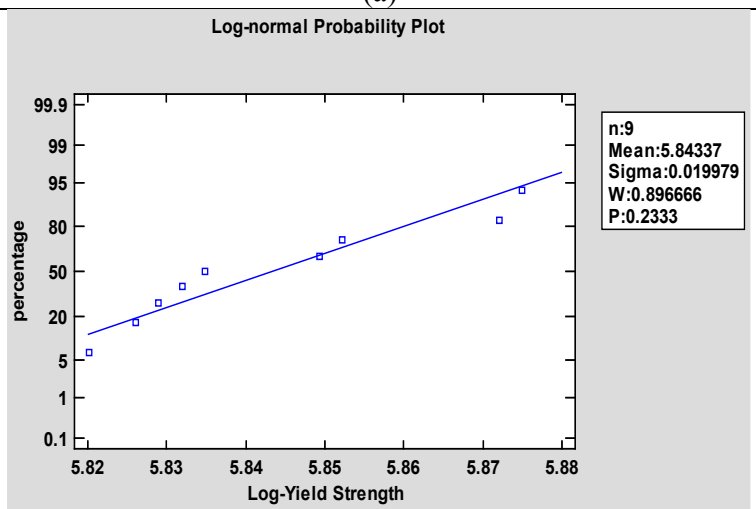

(b)

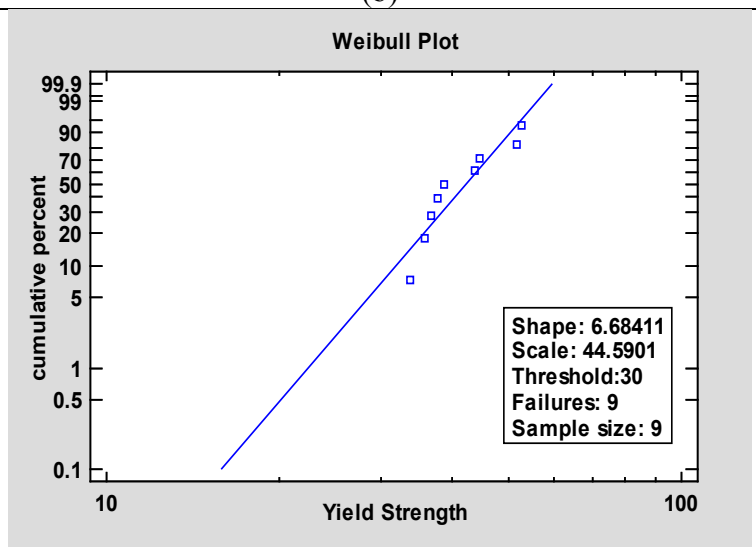

(c)

Figure 5.1 The Probability plot for Yield strength (a) Normal (b) Lognormal and (c) Weibull.

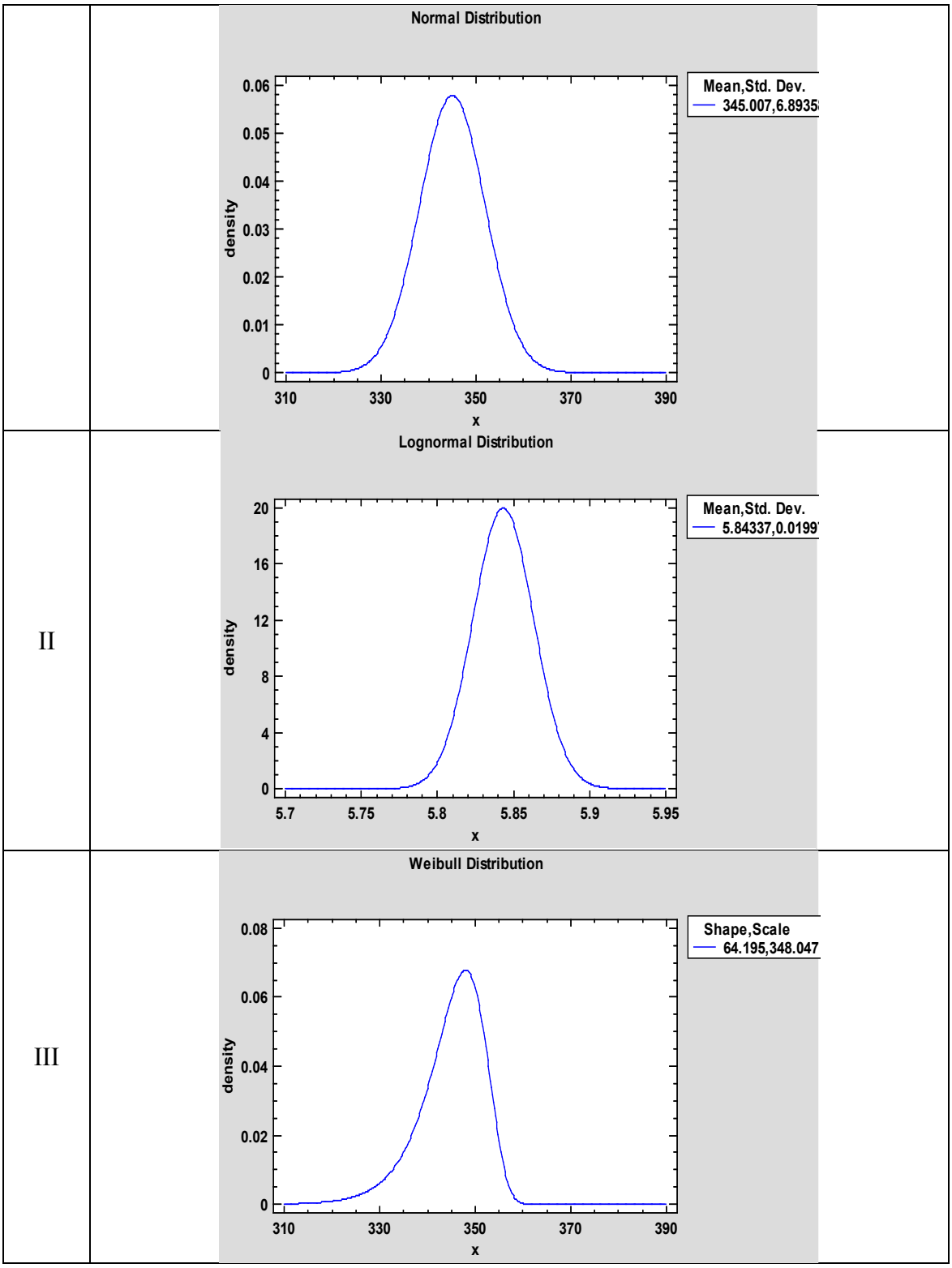

II

III

Figure 5.2 Distributions for Yield Strength (I) Normal (II) Lognormal and (III) Weibull.

Table 5.3 Distribution Summaries for Yield Strength.

Normal	Lognormal	Weibull
mean = 345.007	mean = 345.0	shape = 64.195
standard deviation = 6.89358	standard deviation = 6.9282	scale = 348.047
	Log scale: mean = 5.84337	
	Log scale: standard deviation = 0.019979	

5.3.2 Ultimate Tensile Strength

Table 5.4 show the statistical summary for ultimate tensile stress obtained through conducting static test for the cast specimens.

Table 5.4 Statistics Summary for Ultimate Tensile Strength.

Mean	553.111
Standard deviation	13.4019
Coefficient. of variation	2.423%
Standard skewness	1.56723
Standard kurtosis	1.98651

The coefficient of varation for tensile strength computed above in table 5.5 results in a quite consistent product as it shows a 2.4 %, which is a small variation in Tensile strength.

Normal, lognormal and Weibull distribution models are valid to characterize variability for Tensile strength as they all show P-value greater than 0.05. which is shown in the goodness of fit test, Kolmogorov-Smirnov Test in table5.6. Figure 5.3 show the probability plot for the normal, lognormal and Weibull probability plot respectively, are used to characterize the ultimate tensile strength.

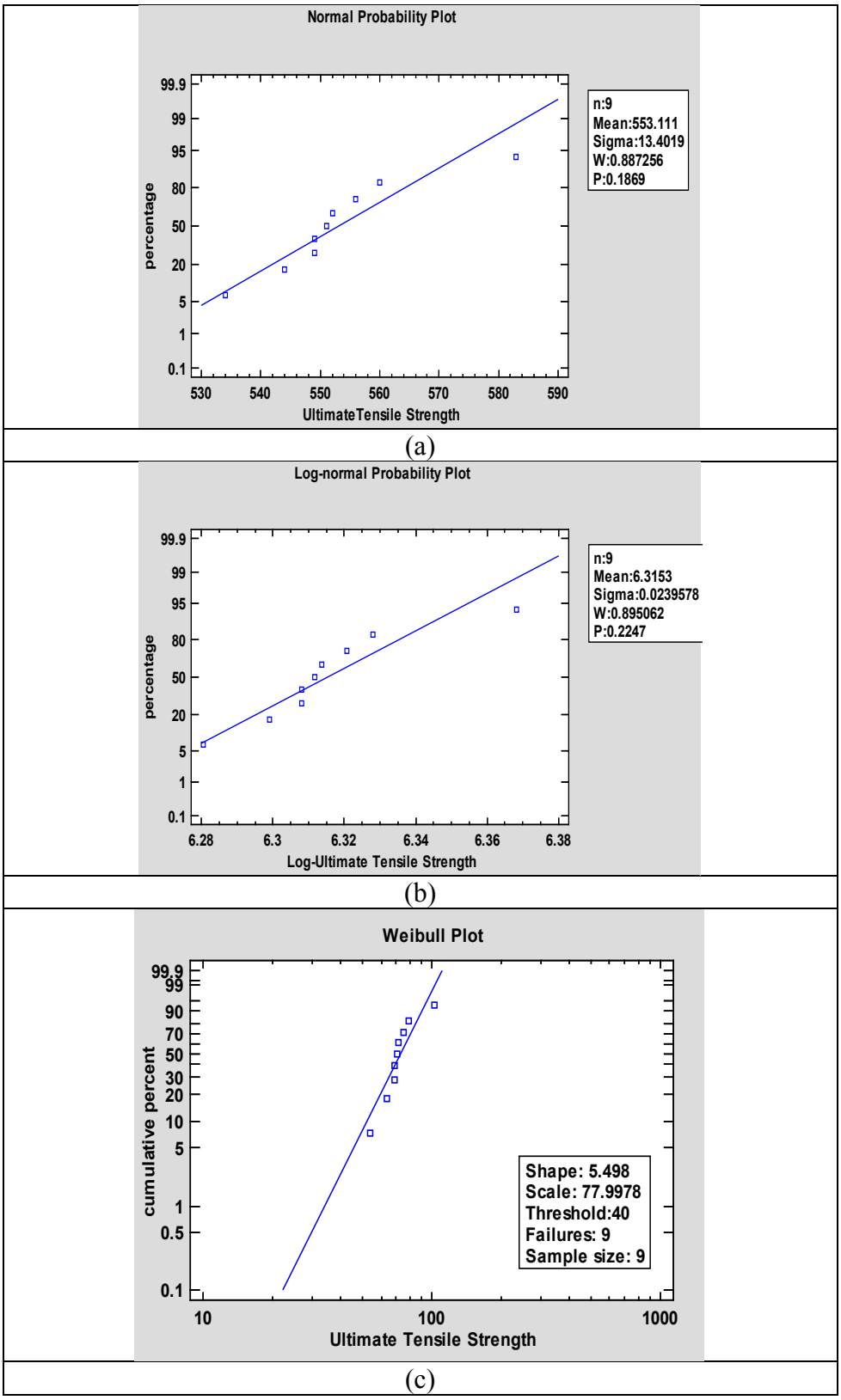

Figure 5.3 The Probability Plot for Ultimate Tensile Strength (a) Normal (b) Lognormal and (c) Weibull.

Table 5.5 Goodness-of-Fit Tests, Kolmogorov-Smirnov for Ultimate Tensile Strength.

	Normal	Lognormal	Weibull
DPLUS	0.199707	0.195848	0.266023
DMINUS	0.15729	0.159608	0.111039
DN	0.199707	0.195848	0.266023
P-Value	0.865446	0.880332	0.547288

Table 5.6 provides the summary for the proposed distribution which are displayed in figure 5.4 for the Normal, Log-normal and Weibull distribution, respectively.

Table 5.6 Distribution Summaries for Ultimate Tensile Strength.

Normal	Lognormal	Weibull
mean = 553.111	mean = 553.128	shape = 53.5338
standard deviation = 13.4019	standard deviation = 13.2536	scale = 558.948
	Log scale: mean = 6.3153	
	Log scale: standard deviation = 0.0239578	

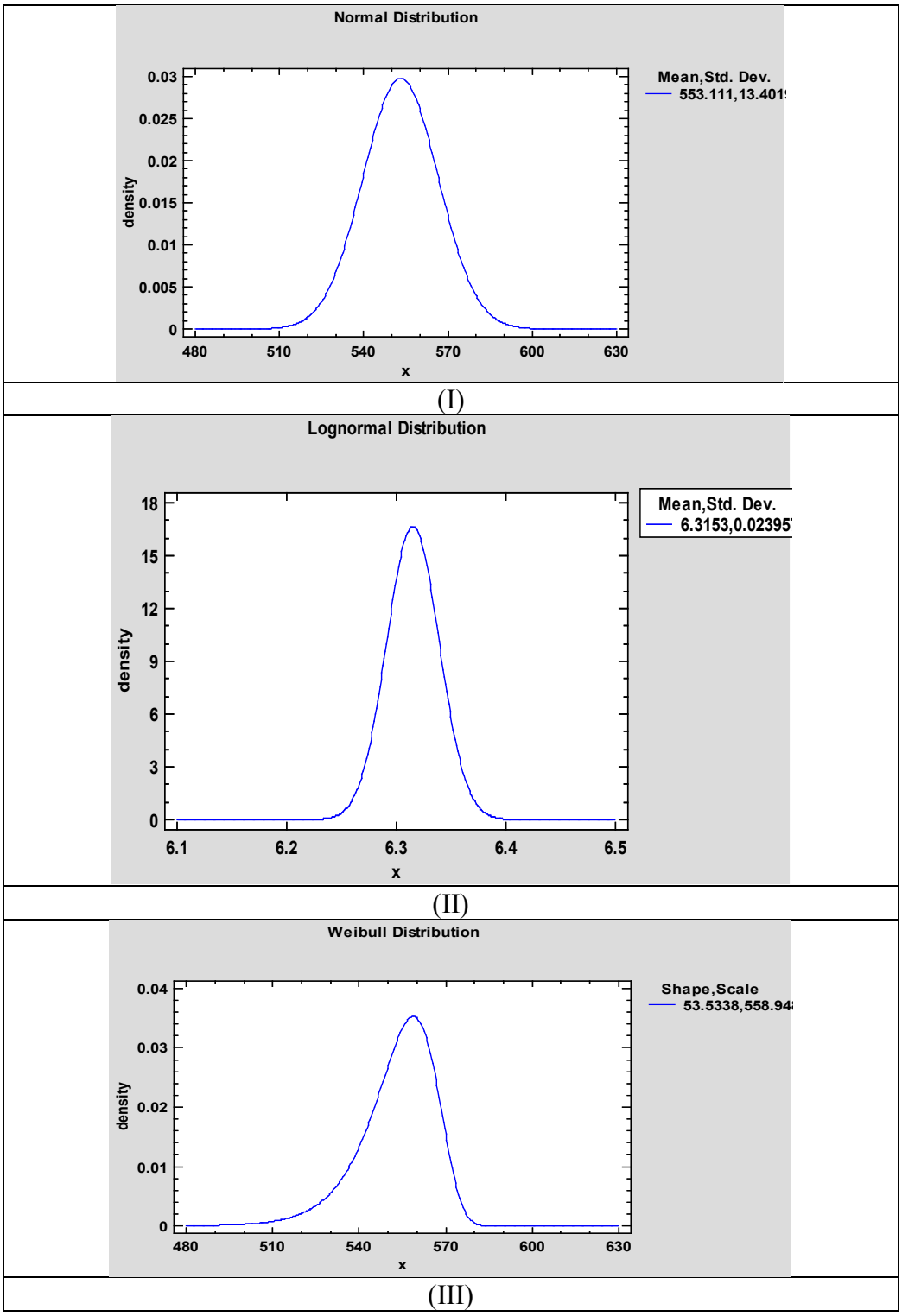

Figure 5.4 Distributions for Ultimate Tensile Strength (I) Normal (II) Lognormal and (III) Weibull.

5.3.3 Elongation

Table 5.7 display statistical summary for Elongation obtained through conducting static test for the cast specimens

Table 5.7 Statistics Summary for Elongation.

Mean	24.8556
Standard deviation	2.35961
Coefficient. of variation	9.49331%
Standard skewness	0.804753
Standard kurtosis	0.0441856

The coefficient of variation in ductility displayed the utmost variability with respect to tensile and yield strength in products, reaching a peak variability value of 9.49 % which around 0.1.

A dissimilarity in temperature between the samples in the mold exists which is highly hypothesized that it is an attributed to differences in the cooling rates that are present amongst the test samples as a consequence; for this reason, ductility varies subsequently. The resulting ductility variation will significantly increase the variability in life of the products.

To fully enhance the reliability of the product, we must ensure that elongation variability is reduced. This can be ensured by thermal cooling analysis of different alternative mold design for the product

All models are valid as they all show P-value greater than 0.05which is demonstrated in the goodness of fit test, Kolmogorov-Smirnov test in table5.8.

Figure 5.5 show the probability plot for the proposed model of the probability models used to characterized elongation.

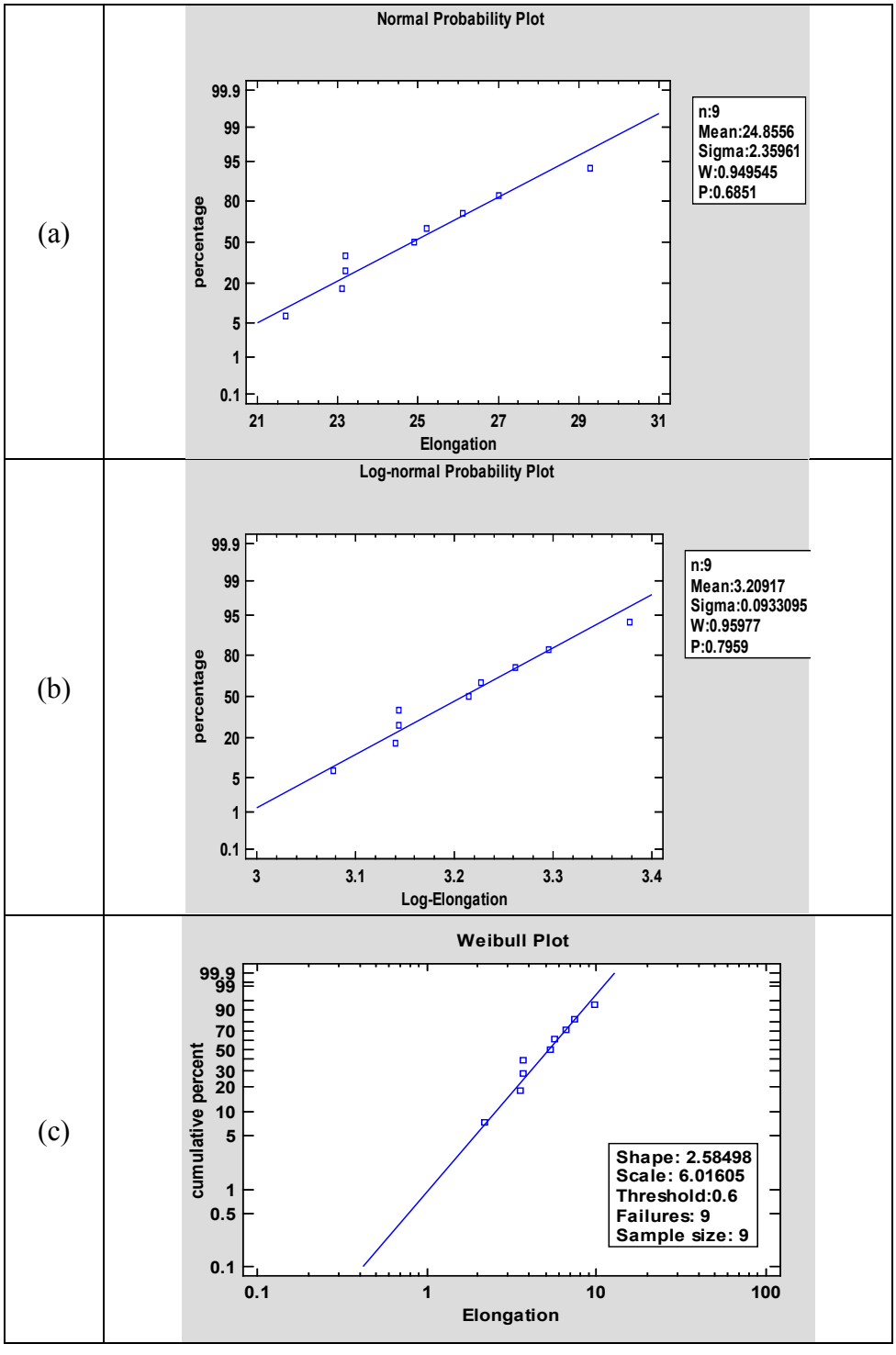

Figure 5.5 The Probability Plot for Elongation (a) Normal (b) Lognormal and (c) Weibull.

Table 5.8 Goodness-of-Fit Tests, Kolmogorov-Smirnov for Elongation.

	Normal	Lognormal	Weibull
DPLUS	0.202988	0.201477	0.192626
DMINUS	0.117326	0.117605	0.130387
DN	0.202988	0.201477	0.192626
P-Value	0.852195	0.858361	0.892151

Table 5.9 display the summary for the suggested distributions which are shown in figure 5.6 for the Normal, Log-normal and Weibull distribution respectively

Table 5.9 Distribution Summaries for Elongation.

Normal	Lognormal	Weibull
mean = 24.8556	mean = 24.8665	shape = 11.1992
standard deviation = 2.35961	standard deviation = 2.32534	scale = 25.9106
	Log scale: mean = 3.20917	
	Log scale: standard deviation = 0.0933095	

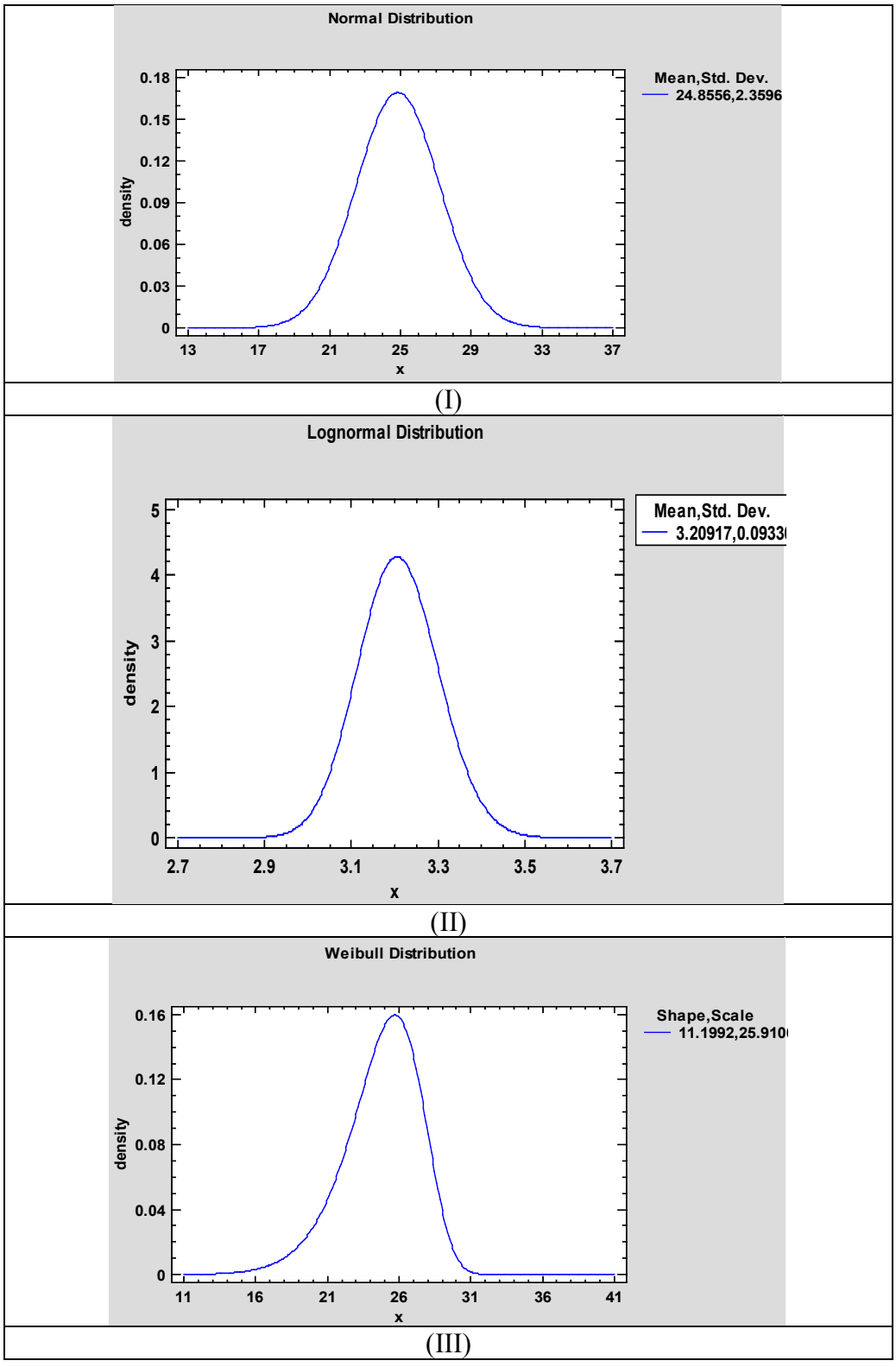

Figure 5.6 Distributions for Elongation (I) Normal (II) Lognormal and (III) Weibull.

5.3.4 Hardness

As for mechanical strength the hardness values have been measured using the Vickers hardness tester.

Table 5.10 Statistics Summary for Hardness.

Mean	88.9686
Standard deviation	2.4238
Coefficient of variation	2.72433%
Minimum	81.3
Maximum	92.9
Range	11.6
Standard skewness	-3.75955
Standard kurtosis	4.16867

The statistics result for Hardness also reveal that the coefficient of variation show the same level or percentage as shown previously in ultimate tensile strength and yield strength. Product seem to be quite consistent. Table 5.11 display the summary for the suggested distributions which are shown in figure 5.7 for the Normal and Log-normal distribution respectively.

Table 5.11 Distribution Summaries for Hardness.

Normal	Normal
mean = 88.9686	mean = 88.97
standard deviation = 2.4238	standard deviation = 2.47636
	Log scale: mean = 4.48791
	Log scale: standard deviation = 0.0278282

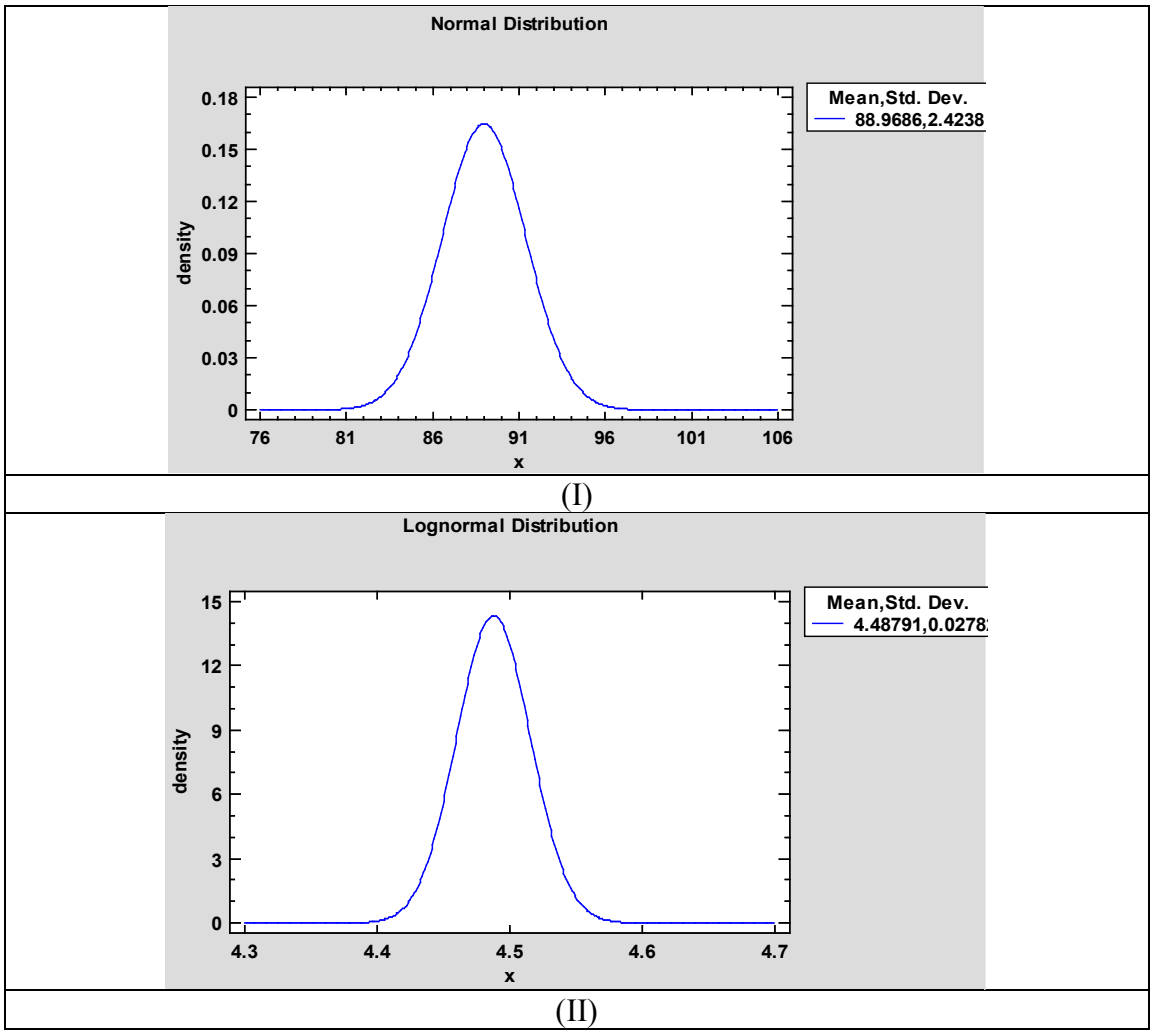

Figure 5.7 Distributions for Hardness (I) Normal and (II) Lognormal.

5.3.5 Conclusion of Static Properties

The total micro porosity in optimized molds is max 1.5% for steel [40]. The quality of the casting through optimized molds are high quality reflected by the low value of coefficient of variation. The greatest scatter is in elongation, so this scatter has direct implication on the crack propagation under fatigue loading. So, we expect a large scatter in fatigue life and that is what we are going to explore in the following section.

5.4 Fatigue Properties

The following figure demonstrate the S-N curve in a log scale.

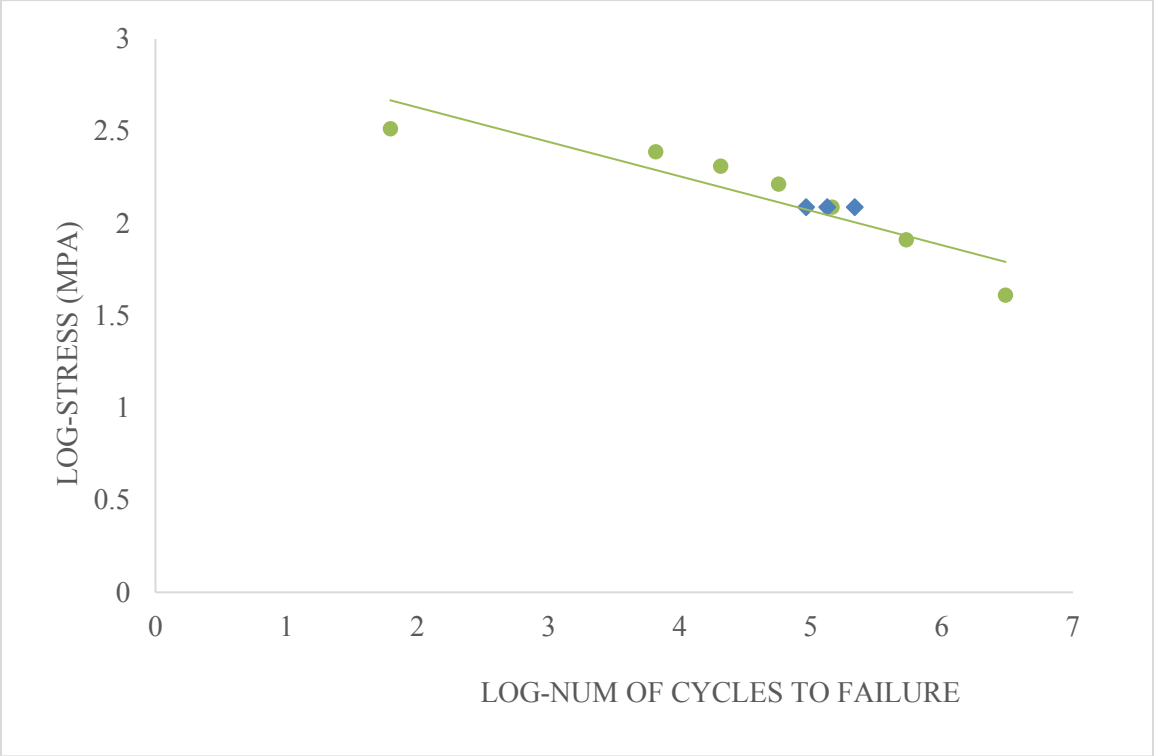

Figure 5.8 Log Scale S-N Curve for Cast Specimen [32]**, The Blue Diamonds are the Author Results.**

Simple regression model has been developed for the prediction of amount of, the relationship between the stress and life in log scale of the fitted result can be described in a linear model as follows:

$$\ln S = 3.38431 - 0.253108 \ln N \quad (5.7)$$

In consideration of the P-value in the Analysis of variance (ANOVA) table 5.12 & 5.13 is less than 0.05, which indicate there is a statistically significant relationship between stress and life at the 95.0% confidence level.

The R-Squared statistic gives an indication that the model, as fitted explains 97.9205% of the variability in stress-log. The correlation coefficient equals -0.989548, demonstrating a

strong relationship among the variables. The standard error of the estimation displays the standard deviation (SD) of the residuals to be 0.0315211. This result value can be utilized to develop prediction limits for new observations. The mean absolute error (MAE) of 0.0227613 is the average value of the residuals. The summary for statistical report for the linear relationship results from the simple regression model is given table 5.12 below

Table 5.12 Summary Table for the Coefficients.

	Least Squares	*Standard*	*T*	
Parameter	*Estimate*	*Error*	*Statistic*	*P-Value*
Intercept	3.38431	0.102235	33.1031	0.0001
Slope	-0.253108	0.0212957	-11.8854	0.0013

Table 5.13 ANOVA Report for the Linear Relationship between Ln Stress and Ln Life.

Source	*Sum of Squares*	*Df*	*Mean Square*	*F-Ratio*	*P-Value*
Model	0.140355	1	0.140355	141.26	0.0013
Residual	0.00298074	3	0.00099358		
Total (Corr.)	0.143336	4			
Correlation Coefficient = -0.989548 R-squared = 97.9205 percent R-squared (adjusted for d.f.) = 97.2273 percent Standard Error of Est. = 0.0315211 Mean absolute error = 0.0227613 Durbin-Watson statistic = 1.41644 (P=0.0354) Lag 1 residual autocorrelation = 0.0178783					

The Durbin-Watson (DW) statistic tests the residuals to determine if there is any significant correlation based on the order in which they occur in our data file. Since the P-value is less than 0.05, there is an indication of possible serial correlation at the 95.0% confidence level. The Table 5.14 below shows 95% confidence intervals for the coefficient in the model. Confidence intervals show how precisely the coefficient can be estimated given the amount of available data and the noise which is present. In addition to the best predictions, the table

and figure 5.8 show that 95.0% prediction intervals for new observations and 95.0% confidence intervals for the mean of many observations

Table 5.14 Confidence Intervals for the Predicted Values in the Model.

		95.00%		*95.00%*	
	Predicted	*Prediction*	*Limits*	*Confidence*	*Limits*
X	*Y*	*Lower*	*Upper*	*Lower*	*Upper*
3.81591	2.41847	2.29149	2.54546	2.34061	2.49633
5.72881	1.9343	1.80612	2.06249	1.8545	2.01411

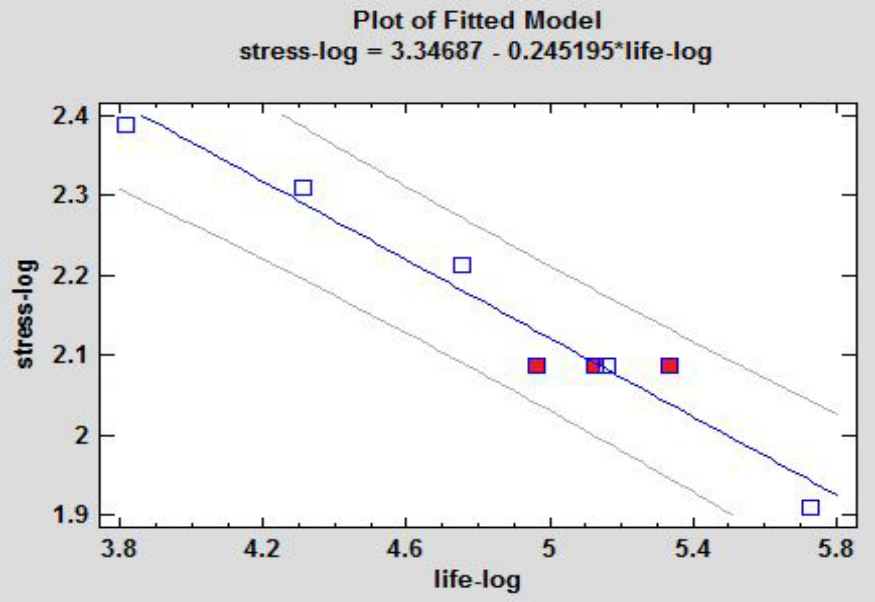

Figure 5.9 Plot of Fitted Model show the 95% Confidence Interval.

5.4.1 Conclusion of Fatigue Properties

The experimental results in form of SN diagram with 95% confidence level with a single realization show that the relationship is logarithmic with a = value and b = value. We can repeat the same realization and get a family of curves. We have not done that, but this is available in literature. We use 95% confidence limit and then verify that with three additional data points at a single load level that validates the assumption. This estimated scatter is outcome of the static properties scatter and can be represented by the three distributions i.e. normal lognormal and Weibull.

CHAPTER 6

EFFECT OF MICRO POROSITY ON FATIGUE LIFE

6.1 Introduction

Porosity in castings can be classified in two main groups (macro porosity and micro porosity) based on scale and formation mechanism. Macro porosity is usually having a large size and forms when a liquid that is surrounded with a solidified material. The order of magnitude of the developing pore/cavity depends on the volume of encircled liquid and the shrinkage amount combined with the phase alteration from liquid to solid. Macro porosity is rectified via appropriate risers and gates within the mold and/or utilizing exothermic and/or chills to supervise the solidification development.

In contrast, micro porosity forms inter dendritically at the microstructure scale. Hence, its formation is mechanically more intricate, harder to forecast, and usually harder to mitigate. Micro porosity can influence fatigue resistance extremely, yet, it may not lead to much localized stress accumulation and stress redistribution [8],[40], [41], [44].

The ASTM standard casting radiographs,[37],[45], [46] explain only the 'qualitative' porosity amount permitted in a casting.

The most popular approaches utilized to estimate fatigue life of castings, using porosity, are: first approach is modeling pores as "equivalent" cracks or notches and finding the local strain emerging from the result of the notch and applying the concepts of strain-life to anticipate the life of fatigue. This approach is occasionally called "crack initiation" life

prediction. Employing this prediction scheme singly supposes that crack initiation engrosses most of the fatigue life.

2) Pre-existing cracks inside the element are used to model the porosity and utilizing linear elastic fracture mechanics (LEFM) to predict crack growth.

Component life predictions utilizing the second approach presume crack propagation engrosses most of the life. Incorporating both schemes of prediction generates the so-called "total life" of the component, which is the summation of the life of initiation and propagation [41].

6.2 Used Objective and Approach

It is obvious that despite the cast specimen which are "radiographic sound"; the micro porosity has a degrading effect on the fatigue life. It is quite common to estimate the effect of micro porosity through detailed finite element analysis approach. This approach however requires heavy simulation and computational efforts and cannot be achieved for a quick estimation of decrease in fatigue life.

The main goal of this section is to present a simple analytical approach to predict the effect of micro porosity on fatigue life of parts which are casted using optimized mold.

The approach is more analogous to Marin factors that predict the fatigue life of any part which deviates from the standard test conditions. Marin factors are just the correction factors which are applied as follows [47]:

$$\boldsymbol{S_e = k_a k_b k_c k_d k_e k_f S'_e} \qquad (6.1)$$

where

S'_e : the endurance strength of a sound specimen

S_e : the endurance strength of a part under actual geometry and conditions of operation.

k_a : account for the difference of surface finish. It can be represented by $k_a = \mathrm{a}(S_{ut})^b$ where (S_{ut}) is the minimum tensile strength, (a) and (b) are found from [39].

k_b: size factor, for axial loading =1.

k_c**:** load factor, for axial loading =0.85.

k_d **:** temperature factor, for room temperature = 1.

k_e **:** Reliability factor, Since fatigue specimens in present work were prepared using ASTM E-466 [37] procedure standard and fatigue testing is conducted according to above mentioned specified standard ,for standard test condition =1.

k_f miscellaneous effects, we take it for porosity factor and denote it by k_p**.**

The next relationship is frequently used, if the endurance strength is not available from a fatigue test[39].

$$\boldsymbol{S'_e = 0.5\, S_{UTS}} \quad (6.2)$$

Where S_{UTS} : the ultimate tensile strength.

Substitute equation (6.2) in equation (6.1), equation (6.1) can be written as follow:

$$\boldsymbol{S'_e = k_a k_b k_c k_d k_e k_p\, 0.5\, S_{UTS}} \quad (6.3)$$

Where S_e and S_{ut} are the ultimate tensile strength and endurance strength of a cast specimen with microporosity respectively.

$k_b = k_d = k_e = 1$, $k_c = 0.85$ as mentioned before

$k_a = a(S_{ut})^b$. For machined surface finish from reference [39] a=4.51MPa, b=-0.265 and from experimental results in chapter 4 $S_{ut} = 534\,MPa$ by calculating these value k_a=0.853.

By substituting the values of Marin factors in equation (6.3). It can be written as follow:

$$\boldsymbol{S_e = (0.853 * 1 * 0.85 * 1 * 1 * K_p) * (0.5)\ S_{UTS}} \qquad (6.4)$$

Next the porosity factor can be estimated based on the analytical approach for producing the SN diagram, which were presented in Chapter 3 for developing the sound material diagram. For the sake of convenience, the relevant equations are presented again the following. Only the equation related to high cycle fatigue are presented because for all practical engineering applications, the expected fatigue life will always be in high cycle range.

Equation (6.5) show the relationship between the S and N in high cycle region and it is valid for two conditions, firstly number of cycles is more than one thousand and less than one million cycles and secondly the stress is between the value of stress at one thousand and endurance limit of the material.

$$\boldsymbol{S = a\,N^b} \qquad (6.5)$$

The values for coefficient *a* and exponent *b* are calculated as shown below in equations (6.6) and (6.7) respectively [39]:

$$\boldsymbol{a} = \frac{(\boldsymbol{f}\,\boldsymbol{S_{UTS}})^2}{\boldsymbol{S_e}} \quad (6.6)$$

$$\boldsymbol{b} = -\boldsymbol{1/3}\ \boldsymbol{log}\left(\frac{\boldsymbol{f}\,\boldsymbol{S_{UTS}}}{\boldsymbol{S_e}}\right) \quad (6.7)$$

Substitute equation (6.3) in equation (6.6) yields:

$$\boldsymbol{a} = \frac{(\boldsymbol{f}\,\boldsymbol{S_{UTS}})^2}{\boldsymbol{K}\,\boldsymbol{S_{UTS}}}$$

So

$$\boldsymbol{K} = \frac{(\boldsymbol{f}\,\boldsymbol{S_{UTS}})^2}{\boldsymbol{a}\,\boldsymbol{S_{UTS}}} = \frac{\boldsymbol{f^2}.\boldsymbol{S_{UTS}}}{\boldsymbol{a}} \quad (6.8)$$

Let us call *K* value by using (6.8) as $K_{p,a}$ is porosity correction factor resulting from coefficient a. Another *K* value could be found by using (6.3) and (6.7) as $K_{p,b}$ is porosity correction factor resulting from exponent b. Substitute equation (6.3) in equation (6.7)

$$\boldsymbol{b} = -\boldsymbol{1/3}\ \boldsymbol{log}\left(\frac{\boldsymbol{f}\,\boldsymbol{S_{UTS}}}{\boldsymbol{K}\,\boldsymbol{S_{UTS}}}\right)$$

So

$$\boldsymbol{K} = \frac{\boldsymbol{f}}{\boldsymbol{10^{-3b}}} \quad (6.9)$$

Equation (6.8) and (6.9) provide two alternate analytical expression for the porosity factor *K*. The next section shows the estimation of porosity factor for our material that is used cast specimen manufactured to conduct this work.

6.3 ASTM A216 WCB Steel

The coefficient *a* and exponent *b* for the cast specimen can be obtained by using a power curve fitting of the form equation (6.5) on the experimental data of Figure 4.14. The parameter *f* can be obtained by substituting N = 10^3 in the fitted power curve. The fitted curve for the cast specimen experimental data and the curve for the sound specimen are shown in Figure 6.1

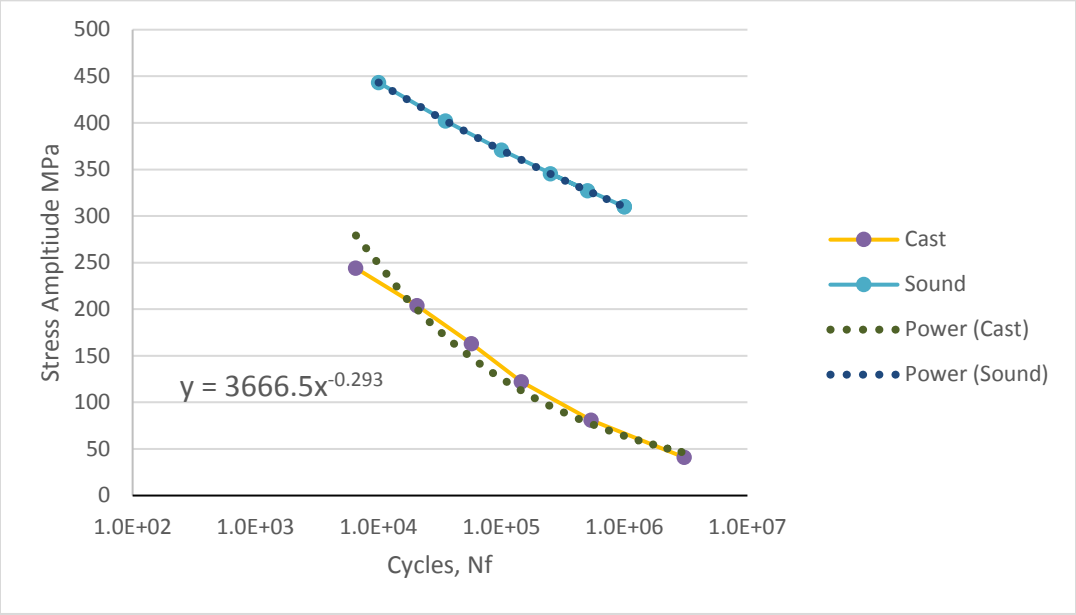

Figure 6.1 Sound versus Actual SN Data for the Steel.

The values of the parameters on right hand side of equation (6.8) and (6.9) are shown in Table 6.1 below

Table 6.1 Properties Obtained from Experimental for ASTM A216.

ASTM A216 WCB Steel		
Ultimate Tensile Strength , S_{UTS}	MPa	549
Modulus of Elasticity, E	GPa	191
the fatigue strength fraction, f	-	0.88
a	MPa	3666.5
b	-	-0.293

So

$$K_{p,a} = \frac{f^2 . S_{UTS}}{a} = \frac{(0.882)^2 \times 549}{3666.5} = 0.1166 \quad (6.10)$$

$$K_{p,b} = \frac{f}{10^{3b}} = \frac{0.882}{10^{(-3 \times -0.293)}} = 0.1166 \quad (6.11)$$

The values of $K_{p,a}$and $K_{p,b}$ obtained above as shown are identical and equal to 0.117.i.e::To obtain the value of K by substituting in equation (6.4) where $K_{p,a}$and $K_{p,b} = K$ so it will be

$$K_p = K_{p,a} \& K_{p,a} = 0.117 \quad)6.12)$$

So, the value of K equals 0.117. And for our radiographic sound specimen by using equation (6.4) and substituting the calculated value of K above in equation (6.12)

$$S_e = 0.0423\, S_{ut} \quad (6.13)$$

To validate the approach presented above the factor *K* is also estimated for the data presented by Sigl et al [40]. The SN diagram for their material is shown in Figure 6.2. The curves for the sound and micro porosity in Figure 6.2 were then digitized to use a curve fitting to obtain the values of parameters *a*, *b* and *f*. The digitized curve and the associated curve fitting are shown in Figure 6.3 The corresponding values of parameters are summarized in Table 6.2.

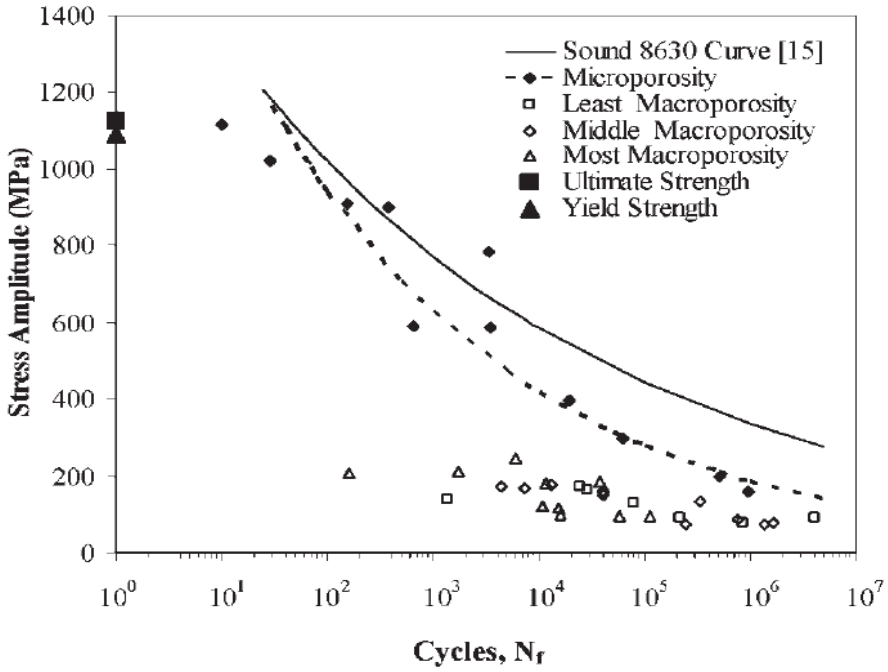

Figure 6.2 S-N Curve for 8630 Cast Steel with Different Quality of Porosity [40].

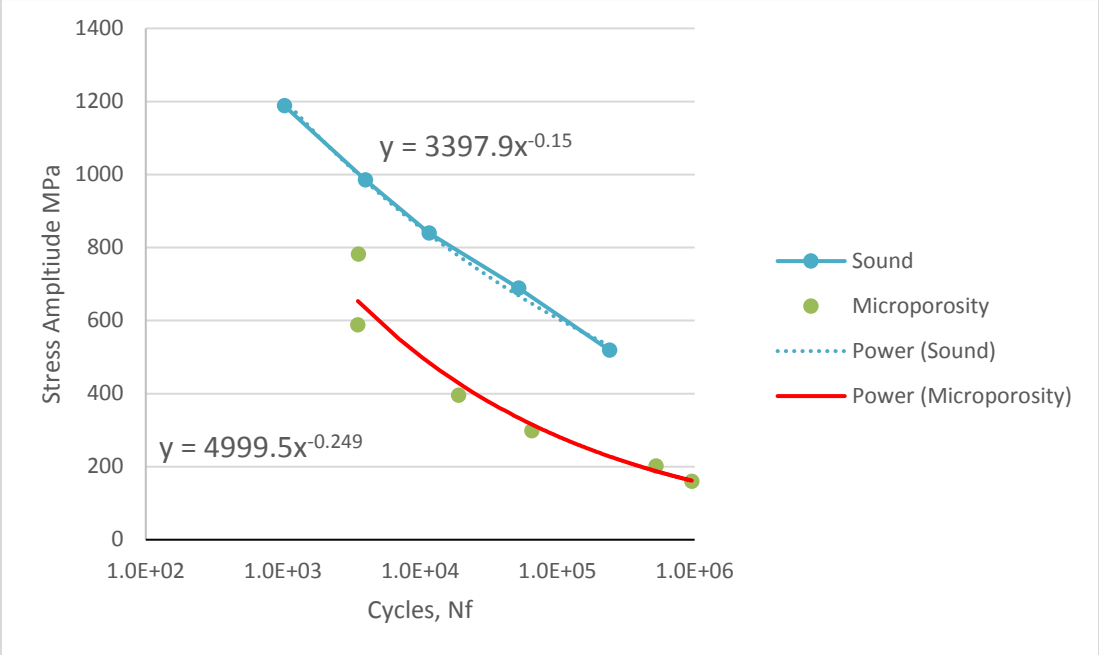

Figure 6.3 The Digitized Curve and the Associated Curve Fitting for 8630 Cast Steel.

Table 6.2 Properties of 8630 Steel for Micropore Material [40]**.**

Micropore Material		
Ultimate Tensile Strength , S_{UTS}	MPa	1125
Modulus of Elasticity, E	GPa	197
the fatigue strength fraction, *f*	-	0.79
a	MPa	4999.5
b	-	-0.249

The porosity factor can now be estimated as follows:

$$K_{p,a} = \frac{f^2.S_{UTS}}{a} = \frac{(0.79)^2 \times 1125}{4999.5} = 0.1404$$

$$K_{p,b} = \frac{f}{10^{3b}} = \frac{0.79}{10^{(-3\times-0.249)}} = 0.1414$$

As before, it can be observed that the porosity factor from two expressions is in good agreement with each other. Also, the K value is very closed to the one for our material i.e 0.117. Thus, this validates the developed approach of porosity factor *K*.

Next we compare the prediction of fatigue life based on porosity factor *K* with the one obtained through detailed analysis based on casting and finite element simulations., Khan[32] predicted the fatigue life of the cast specimen with micro porosity (cf. Figure. (4.14)) using detailed analysis procedure described in the previous chapter. The results of the presented analytical approach (cf. Eq. (6.8 and 6.9)) and the ones obtained by Khan are compared with the actual experimental results in Figure 6.4.

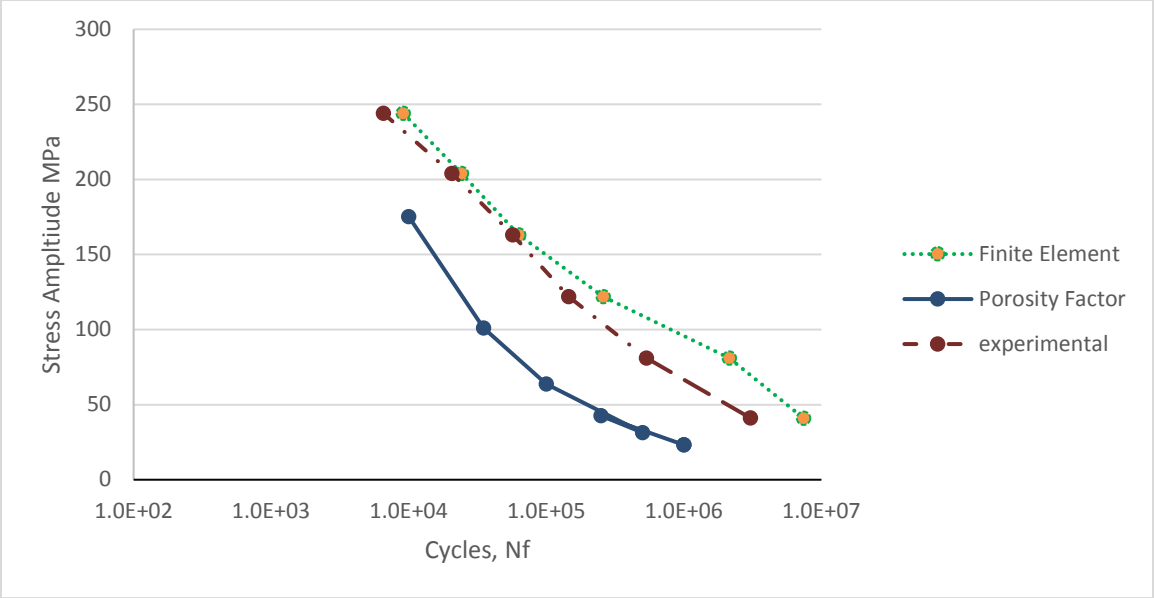

Figure 6.4 Comparison of Experimental Fatigue Life with the Life predicted through Finite Element Approach by Khan [32] and Analytical Approaches.

It can be seen that both the finite element and porosity factor approach are giving an excellent prediction of the fatigue life in comparison with actual experimental results of radiographic sound specimen.

Nevertheless, the value of porosity factor is based on the very same experimental results against which it is compared, whereas the finite element results are independent of experimental results and are based on complete virtual experiments. The validity of porosity factor approach is however validated by estimating its value for similar experimental results available in the literature, and it is observed that the porosity factor value ranges from 0.1 to 0.15. Indeed, this range can further be refined by conduction more experimental or virtual experiments. Moreover, due to long time duration required for the fatigue experiments to construct an SN diagram, only one specimen is tested at each load level, which makes the fatigue life as a deterministic variable. It is obvious that the fatigue life is definitely a random variable with a probability distribution function. This requires

testing multiple specimen at each load level to identify the scatter as well as the probability distribution function. This was shown in the previous chapter of the presented work

6.4 Conclusion

The porosity defect of the castings is minimized by using optimized molds designed based on numerical simulation of the casting process. The castings are radiographic sound, nevertheless the micro porosity is uniformly distributed over the entire casting and decreases the static and fatigue strength of the castings. Experimental studies are carried out to evaluate the effect of micro porosity on the static and fatigue strength of the radiographic sound cast specimen. Multiple specimens are tested under static loading to identify the scatter and probability distribution function for yield strength, ultimate tensile strength, and elongation. It is found that all three static properties can be described by any of the three, normal, lognormal or Weibull distributions. It is also observed that all static properties are less than the corresponding sound specimen, manufactured through hot rolling process.

The fatigue tests are conducted with only one specimen is tested at each load level to establish a single SN diagram of the cast specimen. The experimental SN diagram of the corresponding sound specimen is not available in the literature, therefore its developed based on theoretical model available in the literature. The comparison of the sound with cast specimen showed a considerable decrease in the fatigue life due to micro porosity. A theoretical approach is developed to get a very quick estimation of fatigue life with micro porosity. The approach is based on defining a life modification factor called “micro porosity factor” which is applied to estimate the decrease in endurance strength of a cast

specimen. A complete SN diagram is then developed based on analytical approach already available in the literature. The approach is validated by comparing the results with the experimental and detailed numerical approach results.

CHAPTER 7

RELIABILITY ASSESSMENT

7.1 Introduction

The importance and requirement of reliability has increased in the past few years in manufacturing as consequence of the need for expanding sales, achieving higher end-user satisfaction, improve safety of the products and to reduce the cost of maintenance and warranty.

The reliability of a product or a system can be well-defined as the likelihood that, according to defined set of operation conditions, the part or a system will perform its proposed function effectively for a specified interval of time[48].

It is a recognized fact that seemingly identical parts functioning under alike circumstances fail at different points in time. This leads to a necessity to describe failure phenomena in probabilistic terms and consequently, fundamental characteristics of reliability profoundly depend on concepts from probability. Reliability analysis is can be precisely described as the study on the way of how parts, products, things etc. fail.

This chapter delivers the approaches for measuring and quantifying the reliability of cast parts produced as part of the current work.

7.1.1 Basic Reliability formulation

The probability of failure is a function of time can be expressed by

$$P(\mathbf{t} \leq t) = F(t), t \geq 0$$

where, $\mathbf{t}$ is a random variable representing the required time to failure. Thus, (t) is the likelihood that the system or product will fail by time. Then again, (t) is the failure distribution function. Then, the reliability of the part that it will perform the desired function at a certain time is given by

$$\mathrm{R(t)} = 1 - \mathrm{F(t)} = \mathrm{P}(\mathbf{t} > \mathrm{t})$$

where, $R(t)$ is the reliability function. If the random variable namely time to failure $\mathbf{t}$ has a density function (t), then

$$\mathrm{R(t)} = 1 - \mathrm{F(t)} = 1 - \int_0^t \mathrm{f}(\tau)\mathrm{d}\tau = \int_t^\infty \mathrm{f}(\tau)\mathrm{d}\tau$$

7.2 Interference Theory

In a classical strength-limited design, once the criterial of failure is identified, the governor rule for an acceptable design is strength should be greater than stress and to cover uncertainties a design safety factor could be applied

The fundamental idea behind the design factor is to save mean strength and mean stress adequately separated to guarantee the required level of safety in design. Nevertheless, there are issues in using the design factors. The inherent variability of strength and strength factors and of stress and stress factors leads to the idea of stress and strength distributions. Figure 6.1 display the possibility to estimate the competence of a component If the distributions of strength and stress are recognized from the interference.

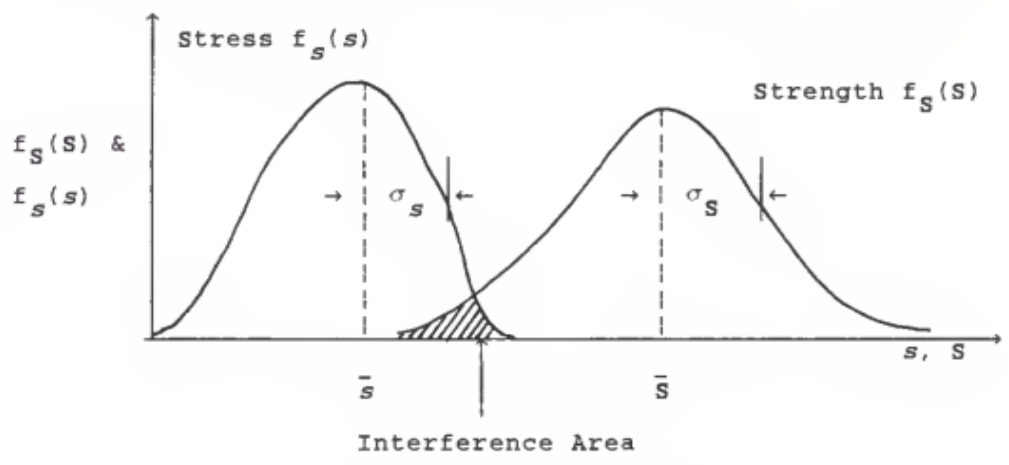

Figure 7.1 The Interference between Stress and Strength once the Mean Strength Surpasses the Mean Stress[49]**.**

The curves in Figure 7.1 represents the interaction of stress and strength distributions when the mean strength exceeds the mean stress and it shows a finite incidence of failure, which is represented by the intersected region.

For a strength-limited design, consider the density function for the strength is f_1 and that for stress is f_2, So the reliability function will be a combined probability function, where

$$P[S > \sigma] = P[S - \sigma > 0] \geq R$$

$$\mathbf{R} = \int_{-\infty}^{\infty} \boldsymbol{f_1(S)} \left[\int_{s}^{\infty} \boldsymbol{f_2(\sigma) d\tau} \right] \mathbf{dS}. 7.1)$$

where, S is the significant strength and σ is the significant load-induced stress. The task for a given design is to ensure that $S>\sigma$.

Figure 7.2. show the stress-strength model which is introduced above, for a typical problem of reliability in fatigue analysis. The components or products are considered safe until the strength and stress distributions are separated with a safety margin, nevertheless, failure of

components is expected when the two distributions begin to intersect as displayed in the unsafe region.

The reliability analysis of the cast specimens exposed to cyclic loading can be categorized according to variation of stress applied with time to

a) Time independent load-induced stress
b) Time dependent load-induced stress

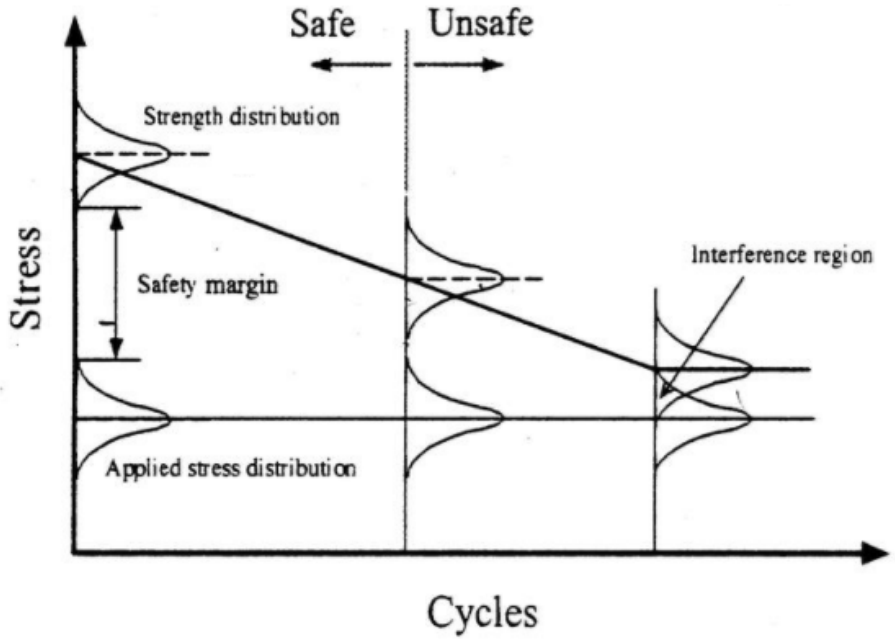

Figure 7.2 The Applied Fatigue Stress-Strength Interference Model [50].

In equation (7.1), noted that S is a function of N and also may be a function of N, So the resulting reliability will be a function of N. Therefore, it will not be statistic reliability, it will be a dynamic reliability, so the generated reliability curve will be dynamic. This equation noting that S is a function of N can be evaluated easily when both (S and σ) quantities are normal distributed or log normal distributed.

The result of normal-normal distributed are shown in figure 7.1 as well as the result for lognormal-lognormal which are shown in figure 7.2 with different level of coefficient of variation of strength

For Normal Distribution

$$\boldsymbol{Z} = -\frac{\boldsymbol{\mu_{s-}\mu_{\sigma}}}{\sqrt{\boldsymbol{\sigma_s^2 + \sigma_{\sigma}^2}}} 7.2)$$

$$R = 1 - \Phi(Z)$$

So, the reliability will be as below

$$\boldsymbol{R = 1 - \Phi\left[-\frac{\left(\frac{\mu_s}{\mu_{\sigma}} - 1\right)}{\sqrt{\left(\frac{\mu_s}{\mu_{\sigma}}\right)^2 C_s{}^2 + C_{\sigma}{}^2}}\right]} \quad (7.3)$$

Where $C_s = {}^{\sigma_s}/_{\mu_s}\ and\ C_{\sigma} = {}^{\sigma_{\sigma}}/_{\mu_{\sigma}}$

C_s: the coefficient of variation of strength

C_{σ}: the coefficient of variation of stress

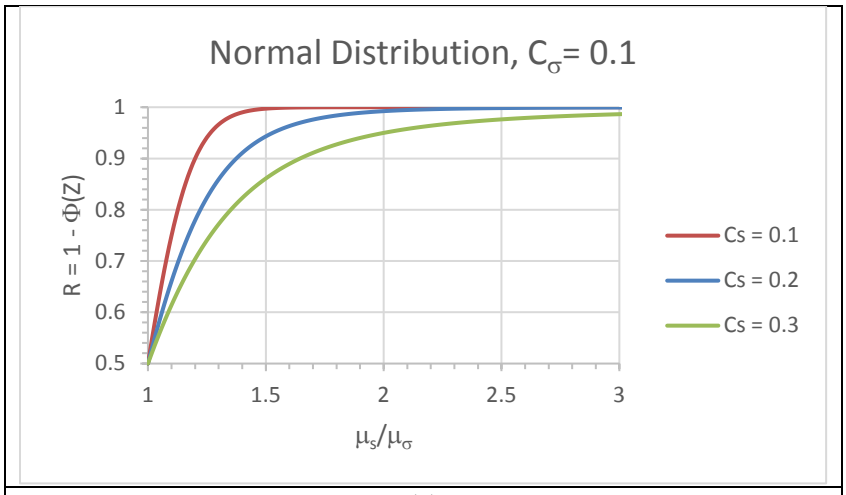

(a)

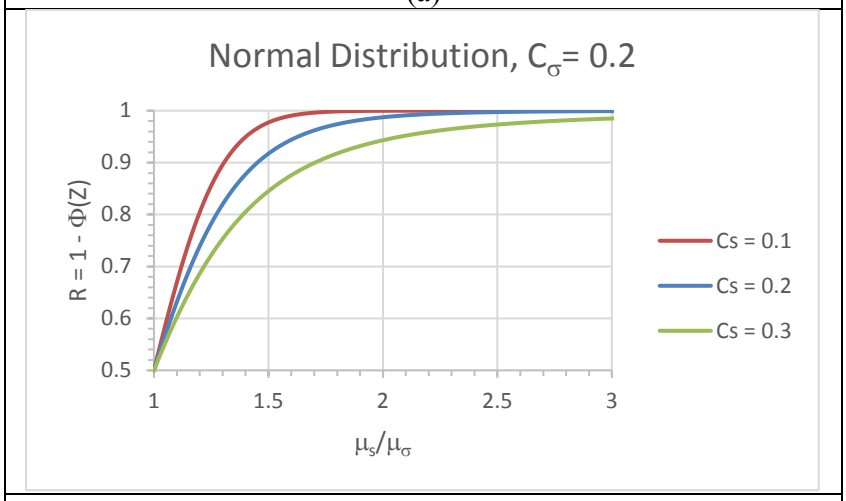

(b)

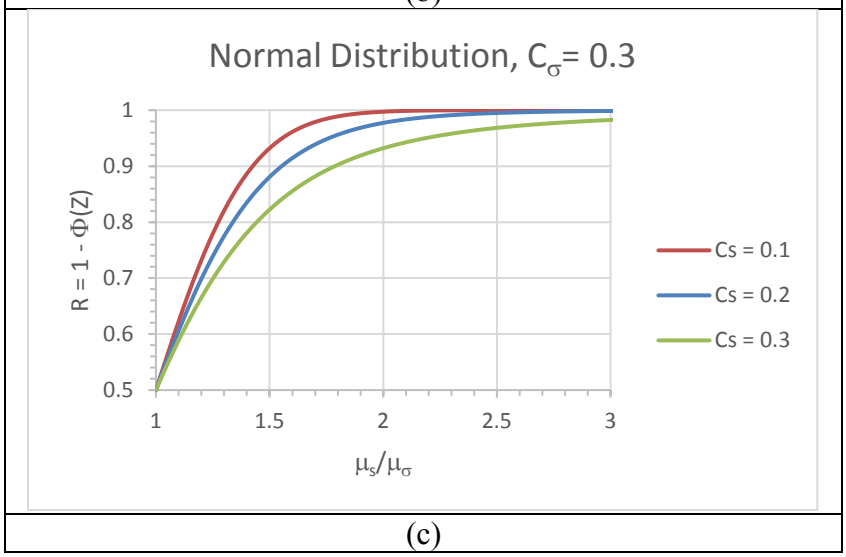

(c)

Figure 7.3 Reliability Function of Scatter in Fatigue Strength for Normal-Normal Distribution.

For Log-Normal

$$\boldsymbol{Z} = -\frac{\boldsymbol{ln}\left(\frac{\boldsymbol{\mu_s}}{\boldsymbol{\mu_\sigma}}\sqrt{\frac{\mathbf{1}+\boldsymbol{C_\sigma}^{\mathbf{2}}}{\mathbf{1}+\boldsymbol{C_s}^{\mathbf{2}}}}\right)}{\sqrt{\mathbf{ln}\left(\mathbf{1}+\boldsymbol{C_s}^{\mathbf{2}}\right)\left(\mathbf{1}+\boldsymbol{C_\sigma}^{\mathbf{2}}\right)}} \quad (7.4)$$

$$R = 1 - \Phi(Z)$$

$$\boldsymbol{R} = \mathbf{1} - \Phi\left[-\frac{\boldsymbol{ln}\left(\frac{\boldsymbol{\mu_s}}{\boldsymbol{\mu_\sigma}}\sqrt{\frac{\mathbf{1}+\boldsymbol{C_\sigma}^{\mathbf{2}}}{\mathbf{1}+\boldsymbol{C_s}^{\mathbf{2}}}}\right)}{\sqrt{\mathbf{ln}\left(\mathbf{1}+\boldsymbol{C_s}^{\mathbf{2}}\right)\left(\mathbf{1}+\boldsymbol{C_\sigma}^{\mathbf{2}}\right)}}\right] 7.5)$$

Where $C_s = {}^{\sigma_s}/_{\mu_s}\ and\ C_\sigma = {}^{\sigma_\sigma}/_{\mu_\sigma}$

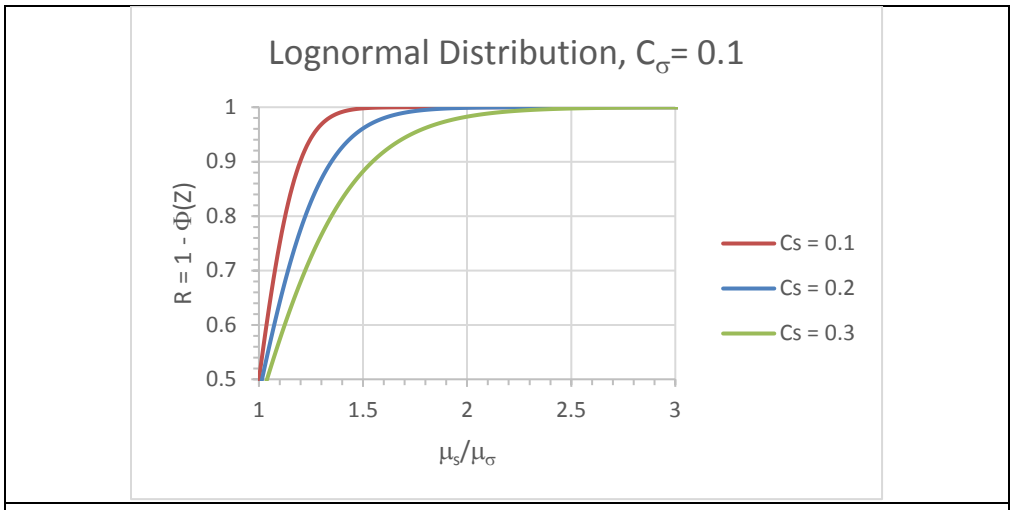

(a)

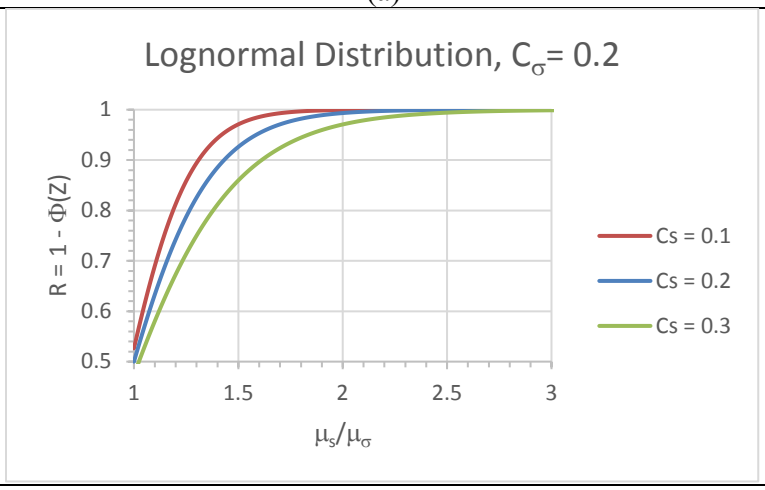

(b)

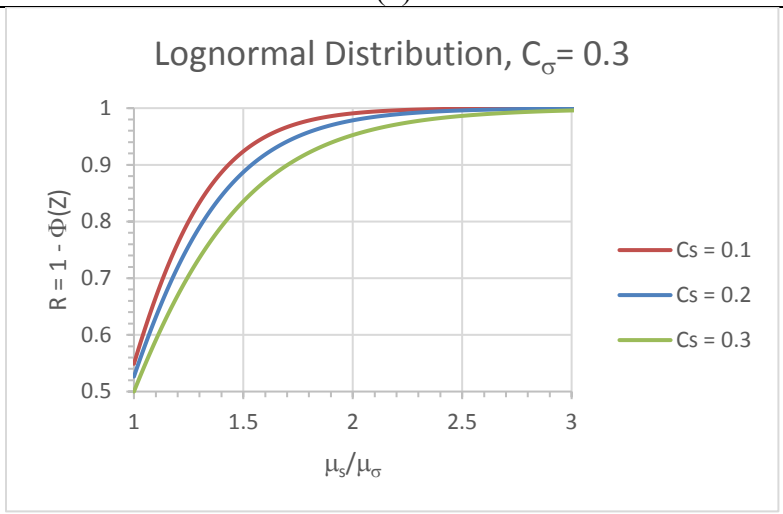

(c)

Figure 7.4 Reliability Function of Scatter in Fatigue Strength for Lognormal-Lognormal Distribution.

To show how to use the above generalized model we consider a system with the strength lognormally distributed, with mean strength = 50 MPa subjected to Time independent stress which is also lognormally distributed, with mean stress= 30MPa. By calculating

$\frac{\mu_s}{\mu_\sigma}$, which is = 1.667 and by using Figure 7.4 for lognormal-lognormal distribution. The effect of the scatter in both strength and stress on the reliability of system is shown in Table 7.1. the system shows the lowest reliability which is 0.88 with scatter 0.3 in both the strength and stress. And the with the same scatter in coefficient of variation of stress 0.3 with more control in the scatter or the variation of the strength, the reliability of the system will reach up to 0.96 when the Cs reach 0.1.

Table 7.1 The Effect of Scatter in Reliability of the System.

	Reliability	Cs
Cσ=0.1	0.999	0.1
	0.987	0.2
	0.934	0.3
Cσ=0.2	0.991	0.1
	0.965	0.2
	0.914	0.3
Cσ=0.3	0.9605	0.1
	0.933	0.2
	0.889	0.3

CHAPTER 8

CONCLUSIONS AND FUTURE WORK

8.1 Conclusions

To conclude this work, the porosity observed in optimized mold was examined by using MAGMAsoft commercial casting software.

we observed that porosity level in a fully optimized mold was at the level of 1 to1.5%, literature also supported that for another similar steel 8630 [40]. Even non-steel products like Aluminum show micro porosity a little higher level[51].

In the study we incorporated this porosity level through a mathematical model, which is empirical model which is a traditional way to look at S/N curve generated from fatigue test and related information, so we use that and added a correction factor for porosity

Then we have used this model to compare the accuracy, of course this information is based up on limited database, but it sounds a promising model even the validation was done.

We utilized the probabilistic characterization of the material earlier and the incorporation of porosity in the S/N curve to generate S/N curve. We created spectrum band on it is average value in which we expected all values will lie if the test is repeated over and over many times. That give some clue of level of variation in the life for given strength and by assuming that the traditionally acceptable models of normal, log-normal and Weibull we can put three further for stress-strength base analysis.

We did that by looking at the stress as a distributed quantity with different coefficient of variation and similarly for different coefficient of variation we set-up the equation for stress- strength interference theory the general equation and specifically for normal- normal interface and for lognormal-lognormal interface we generate reliability curves and for case Weibull -Weibull it is extensive numerical computation needed which can be handle case by case instead of giving close form solution.

Our model is predicting conservative results which are good from a design point of view. We are not challenging the usefulness of FEM approach that is a sophisticated approach help us for learning scientific understanding of the process this is a good approach, but from an engineering point of view the design-based approach as we have developed is also quite useful, more simplified, and quicker to use it without loss of much accuracy.

8.2 Recommendations for Future Work

The foundation of this modeling was built on a limited data and it is a time-consuming for data acquisition.

In the future much, greater amount of data can be generated, and this model can be more refined. In addition to this refining for this model the similar strategy can be developed for ductile cast iron or for Aluminum products which is most commonly used in the cast and will utilized under dynamic loading

References

[1] S. Kalpakjian, S.Schmid, *Manufacturing Processes for Engineering Materials*, Fifth. PEARSON, 2008.

[2] S. L. Nimbulkar and R. S. Dalu, "Design optimization of gating and feeding system through simulation technique for sand casting of wear plate ☪," *Perspect. Sci.*, vol. 8, pp. 39–42, 2016.

[3] M. Blair, R. Monroe, C. Beckermann, R. Hardin, K. Carlson, and C. Monroe, "Designing reliable castings," pp. 63–72, 2005.

[4] C.W.Ammen, *The complete handbook of sand casting*. 1979.

[5] R. Rajkolhe and J. G. Khan, "Defects , Causes and Their Remedies in Casting Process :," vol. 2, no. 3, pp. 375–383, 2014.

[6] N. Fleck, "Metal Foams : a Design Guide Metal Foams : A Design Guide," vol. 3069, no. August, 2014.

[7] R. A. Hardin and C. Beckermann, "Effect of Porosity on the Stiffness of Cast Steel," 2007.

[8] K. M. Sigl, R. A. Hardin, R. I. Stephens, and C. B. Iowa, "FATIGUE OF 8630 CAST STEEL IN THE PRESENCE OF SHRINKAGE POROSITY," no. 3, 2003.

[9] B. Ravi, *Metal casting: computer-aided design and analysis*. PHI Learning Pvt. Ltd, 2005.

[10] B. Ravi, "Computer-aided Casting Method Design, Simulation and Optimization," *Inst. Indian Foundry men*, 2008.

[11] R. A. Hardin and C. Beckermann, "Prediction of the Fatigue Life of Cast Steel Containing Shrinkage Porosity," vol. 40, no. March, 2009.

[12] R. A. Hardin and C. Beckermann, "Effect of Porosity on Deformation, Damage, and Fracture of Cast Steel," *Metall. Mater. Trans. A*, vol. 44, no. 12, pp. 5316–5332, Dec. 2013.

[13] N. Vanderesse, É. Maire, A. Chabod, and J.-Y. Buffière, "Microtomographic study and finite element analysis of the porosity harmfulness in a cast aluminium alloy," *Int. J. Fatigue*, vol. 33, no. 12, pp. 1514–1525, Dec. 2011.

[14] G. Nicoletto, G. Anzelotti, and R. Konečná, "X-ray computed tomography vs. metallography for pore sizing and fatigue of cast Al-alloys," *Procedia Eng.*, vol. 2, no. 1, pp. 547–554, Apr. 2010.

[15] A. du Plessis *et al.*, "Prediction of mechanical performance of Ti6Al4V cast alloy

based on microCT-based load simulation," *J. Alloys Compd.*, vol. 724, pp. 267–274, Nov. 2017.

[16] J. A. Slotwinski, E. J. Garboczi, and K. M. Hebenstreit, "Porosity Measurements and Analysis for Metal Additive Manufacturing Process Control," *J. Res. Natl. Inst. Stand. Technol.*, vol. 119, p. 494, Oct. 2014.

[17] J. Z. Yi, Y. X. Gao, P. D. Lee, H. M. Flower, and T. C. Lindley, "Scatter in Fatigue Life Due to Effects of Porosity in Cast A356-T6 Aluminum-Silicon Alloys," vol. 34, no. September, 2003.

[18] M. Avalle, G. Belingardi, M. P. Cavatorta, and R. Doglione, "Casting defects and fatigue strength of a die cast aluminium alloy : a comparison between standard specimens and production components," vol. 24, pp. 1–9, 2002.

[19] J. Z. YI, X. ZHU, J. W. JONES, and J. E. ALLISON, "A Probabilistic Model of Fatigue Strength Controlled by Porosity Population in a 319-Type Cast Aluminum Alloy: Part II. Monte-Carlo Simulation," *Metall. Mater. Trans. A*, vol. 38, no. 5, pp. 1123–1135, Jun. 2007.

[20] A. ben Ahmed, A. Nasr, A. Bahloul, and R. Fathallah, "An Engineering Predictive Approach of Kitagawa-Takahashi Diagrams of defective A356-T6 alloy considering SDAS dispersion," *Procedia Struct. Integr.*, vol. 5, pp. 524–530, Jan. 2017.

[21] U. A. Dabade and R. C. Bhedasgaonkar, "Casting Defect Analysis using Design of Experiments (DoE) and Computer Aided Casting Simulation Technique," *Procedia CIRP*, vol. 7, pp. 616–621, Jan. 2013.

[22] A. Bahmani, N. Hatami, N. Varahram, P. Davami, and M. O. Shabani, "A mathematical model for prediction of microporosity in aluminum alloy A356," *Int. J. Adv. Manuf. Technol.*, vol. 64, no. 9–12, pp. 1313–1321, Feb. 2013.

[23] R. A. Hardin and C. Beckermann, "Effect of Cooling Rate and Microporosity on Mechanical Performance of a High Strength Steel," no. 5, 2016.

[24] R. Hardin and C. Beckermann, "Effect of Shrinkage on Service Performance of Steel Castings," no. 4, 2002.

[25] K. Mahesh, S. Kulkarni, and R. Gedekar, "Simulation of sand casting to predict porosity for Ductile Iron," 2018.

[26] M. Brůna, D. Bolibruchová, and R. Pastirčák, "Numerical Simulation of Porosity for Al Based Alloys," *Procedia Eng.*, vol. 177, pp. 488–495, Jan. 2017.

[27] M. Unterreiter, G.Wlanis T.Ludwig A.Wu M.Sommitsch, Ch, "Through process of simulation of aluminium A356-Simulation of solidification stress analysis during heat treatment," *Int. J. Multiphys.*

[28] C. Dørum, "Materials & Design Numerical modelling of the structural behaviour

of thin-walled cast magnesium components using a through-process approach," vol. 28, pp. 2619–2631, 2007.

[29] R. A. Hardin and C. Beckermann, "Integrated Design of Steel Castings : Case Studies," no. 2, pp. 1–28, 2009.

[30] H. Search, C. Journals, A. Contact, M. Iopscience, I. O. P. Conf, and I. P. Address, "Integrated design of castings : effect of porosity on mechanical performance," vol. 012069.

[31] J. Olofsson and I. L. Svensson, "Incorporating predicted local mechanical behaviour of cast components into finite element simulations," *Mater. Des.*, vol. 34, pp. 494–500, 2012.

[32] M. A. Khan, "Development of a Simulation-Based Methodology for Mold Design Optimization and Reliability Assessment of Cast Parts," Ph.D Dissertation,Mechanical Engineering department, King Fahad University of Petroleum & Minerals, 2018.

[33] G. A. Hodbe and B. R. Shinde, "Design And Simulation Of LM 25 Sand Casting For Defect Minimization," *Mater. Today Proc.*, vol. 5, no. 2, pp. 4489–4497, Jan. 2018.

[34] C. M. Choudhari, B. E. Narkhede, and S. K. Mahajan, "Methoding and Simulation of LM 6 Sand Casting for Defect Minimization with its Experimental Validation," *Procedia Eng.*, vol. 97, pp. 1145–1154, Jan. 2014.

[35] P. N. Rao, *Manufacturing technology V1*. McGraw Hill Education, 2013.

[36] A. Standard, "E8/E8M, 2009. Standard test methods for tension testing of metallic materials. ASTM international, West Conshohocken PA; 2016. doi: 10.1520," *E0008-E0008M-09, www. astm. org*.

[37] ASTM, "ASTM E466-15," *Stand. Pract. Conduct. Force Control. Constant Amplitude Axial Fatigue Tests Met. Mater. ASTM Int. West Conshohocken, PA, www.astm.org*, 2015.

[38] ASTM, "ASTM A216 / A216M-18," *Stand. Specif. Steel Cast. Carbon, Suitable Fusion Welding, High-Temperature Serv. ASTM Int. West Conshohocken, PA, www.astm.org*, 2018.

[39] R. G. (Richard G. Budynas, J. K. Nisbett, and J. E. Shigley, *Shigley's mechanical engineering design*. McGraw Hill Education, 2010.

[40] K. M. Sigl, R. A. Hardin, R. I. Stephens, and C. Beckermann, "Fatigue of 8630 cast steel in the presence of porosity," *Int. J. Cast Met. Res.*, vol. 17, no. 3, pp. 130–146, Mar. 2004.

[41] R. A. Hardin and C. Beckermann, "Effect of Porosity on Mechanical Properties of 8630 Cast Steel," in *in Proceedings of the 58th Technical and Operating*

Conference, 2004.

[42] R. Winters, A. Winters, and R. G. Amedee, "Statistics: a brief overview.," *Ochsner J.*, vol. 10, no. 3, pp. 213–6, 2010.

[43] Z. Ali and Sb. Bhaskar, "Basic statistical tools in research and data analysis," *Indian J. Anaesth.*, vol. 60, no. 9, p. 662, 2016.

[44] P. Heuler, C. Berger, and J. Motz, "FATIGUE BEHAVIOUR OF STEEL CASTINGS CONTAINING NEAR-SURFACE DEFECTS," *Fatigue Fract. Eng. Mater. Struct.*, vol. 16, no. 1, pp. 115–136, Jan. 1993.

[45] "ASTM E280-15," *ASTM E280-15, Stand. Ref. Radiogr. Heavy-Walled (412 to 12 in. (114 to 305 mm)) Steel Cast. ASTM Int. West Conshohocken, PA, 2015, www.astm.org*, 2015.

[46] "ASTM E186-15," *ASTM E186-15, Stand. Ref. Radiogr. Heavy-Walled (2 to 412 in. (50.8 to 114 mm)) Steel Cast. ASTM Int. West Conshohocken, PA, 2015, www.astm.org*, 2015.

[47] J. Marin, *Mechanical behaviour of engineering materials*. Englewood Cliffs, N.J. : Prentice-Hall, 1962.

[48] M. Sánchez-Silva and G.-A. Klutke, "Reliability of Engineered Systems," 2016, pp. 21–45.

[49] C. R. Mischke and J. E. Shigley, *Standard handbook of machine design*. McGraw-Hill, 1996.

[50] S. Woo, "Introduction to Reliability Design of Mechanical/Civil System," in *Reliability Design of Mechanical Systems*, Cham: Springer International Publishing, 2017, pp. 1–6.

[51] M. Gustavo Waldemar, T. Daniel Oscar, C. Julio César, and G. Aulio César, "Effect of Porosity on the Tensile Properties of Low Ductility Aluminum Alloys," *Mater. Res.*, vol. 7, 2004.

Vitae

Name :Ibrahim Abdelaziz Ali Osman

Nationality :Sudanese

Date of Birth :4/17/1990

Email ibrahim201512090@gmail.com

Address :Sudan- Khartoum- Almamoura-block72-postal code11123.

Academic Background

- :M.Sc. Mechanical Engineering: King Fahad University of Petroleum and Minerals (KFUPM), Dhahran, Saudi Arabia 2019
- B.S Mechanical Engineering: University of Khartoum, Khartoum, Sudan 2011

Experience

- Production Engineer 2012-2015

  DAL Food – SAYGA, Khartoum, Sudan.
- Spare part Engineer 2011- 2012

  Albarajoub Engineering Co.Ltd (BEC), VOLVO CE dealer ,Khartoum, Sudan.

Honors and Awards

- KFUPM's Scholarship - Full scholarship 2015
- Sudan Engineering Society Award for the best performance at graduation project - Mechanical Engineering 2011.

- The university prize for the best graduation project in Mechanical Department for Final year Bachelor Project 2011.

Publication

- **Ibrahim Osman**, A.K.Sheikh, M.A.Khan, J.Albinmousa, S. Pashah "Probabilistic characterization and failure prediction of optimized casting under static and fatigue loads".(Status :Ready to submit)